RE-271

A DIFFUSION MODEL CALCULATION OF THE VARIATIONS PRODUCED IN THE LUNAR ATMOSPHERE BY THE LUNAR MODULE EXHAUST

November 1966

N67-15675

(ACCESSION NUMBER) (THRU)

86 1

(PAGES) (CODE)

30

(NASA CR OR TMX OR AD NUMBER) (CATEGORY)

FACILITY FORM 602

Grumman

RESEARCH DEPARTMENT

GPO PRICE $ _____

CFSTI PRICE(S) $ _____

Hard copy (HC) $ 3.00

Microfiche (MF) 1.30

ff 653 July 65

GRUMMAN AIRCRAFT ENGINEERING CORPORATION

BETHPAGE NEW YORK

Grumman Research Department Report RE-271

A DIFFUSION MODEL CALCULATION OF THE VARIATIONS PRODUCED IN THE LUNAR ATMOSPHERE BY THE LUNAR MODULE EXHAUST†

by

S. N. Milford

and

F. R. Pomilla

Geo-Astrophysics Section

November 1966

†This work was supported in part by the National Aeronautics and Space Administration under Contract NAS 9-4860.

Approved by: Charles E. Mack, Jr.
Charles E. Mack, Jr.
Director of Research

Grumman Research Department Report RE-271

A DIFFUSION MODEL CALCULATION OF THE VARIATIONS PRODUCED IN THE LUNAR ATMOSPHERE BY THE LUNAR MODULE EXHAUST†

by

S. N. Milford

and

F. R. Pomilla

Geo-Astrophysics Section

November 1966

†This work was supported in part by the National Aeronautics and Space Administration under Contract NAS 9-4860.

Approved by: Charles E. Mack, Jr.
Charles E. Mack, Jr.
Director of Research

ACKNOWLEDGMENTS

The authors express their gratitude to Mr. Frank Koch for the use of the results of his calculations of the lunar surface distribution of the LM far-field exhaust gases and for several discussions. They also wish to express their indebtedness to Drs. Leonard Aronowitz and Miriam Sidran for the use of their calculations of surface adsorption coefficients and desorption times. They are grateful to Dr. T. Luzzi and Mr. Daniel Weiss for discussions on the characteristics of near-field LM exhaust gases. Finally, the authors wish to acknowledge the excellent computer programming assistance of Mr. Paul Kalben.

ABSTRACT

A two dimensional diffusion model is developed to study the spread of the exhaust contaminants from the Lunar Module (LM) into the lunar atmosphere. The rarefied ambient lunar atmosphere is treated as an exosphere. The model assumes that the exhaust gas molecules diffuse along the surface as a result of collisions with the surface. The loss mechanisms considered are interactions with the solar wind and solar photons, thermal evaporation, and adsorption to the lunar surface. It is shown that during the LM stay-time, the contamination of the atmosphere is both appreciable and nonuniform in distribution, with the subsequent trend toward a uniform distribution proceeding at different rates for different exhaust gas species.

TABLE OF CONTENTS

Item		Page
I.	Introduction	1
II.	Model Formulation	3
	A. Model I - Time Dependence Only	3
	B. Model II - Space and Time Dependence	8
III.	Atmospheric Source and Loss Mechanisms	22
	A. Source Mechanisms	22
	B. Loss Mechanisms	28
IV.	Results	37
	A. Model I	37
	B. Model II	37
V.	Discussion of Results	39
	A. Model I	39
	B. Model II	41
	C. Approximate Formula	46
VI.	References	50

LIST OF ILLUSTRATIONS

Figure		Page
1	Plot of Equations (5) and (6)	7
2	Path of Integration in the p-plane	14
3	Lunar Coordinate System for Model II	20
4	Pictorialization of the Lunar Atmospheric Source and Loss Mechanisms	23
5	H_2O, H, O_2 — Comparison of Model I Results (Number of Particles/cm^3 versus Time in Seconds) for $J = 10^9$ with $J = 10^{12}$	52
6	O — Comparison of Model I Results (Number of Particles/cm^3 versus Time in Seconds) for Two Different Values of the Parameters τ and J ..	53
7	H_2O — Comparison of Model I Results (Number of Particles /cm^3 versus Time in Seconds) for Two Different Values of the Parameters τ and J	54
8	N_2 — Model I. Variation of LM Exhaust Contamination with Time (Number of Particles/cm^3 versus Time in Seconds) for (a) $J = 10^9$, (b) $J = 10^{12}$	55
9	H_2 — Model I. Variation of LM Exhaust Contamination with Time (Number of Particles/cm^3 versus Time in Seconds) for (a) $J = 10^9$, (b) $J = 10^{12}$	55

Figure		Page
10	CO — Model I. Variation of LM Exhaust Contamination with Time (Number of Particles/cm^3 versus Time in Seconds) for (a) $J = 10^9$, (b) $J = 10^{12}$	56
11	CO_2 — Model I. Variation of LM Exhaust Contamination with Time (Number of Particles/cm^3 versus Time in Seconds) for (a) $J = 10^9$, (b) $J = 10^{12}$	56
12	H — Model I. Variation of LM Exhaust Contamination with Time (Number of Particles/cm^3 versus Time in Seconds) for (a) $J = 10^9$, (b) $J = 10^{12}$	57
13	OH — Model I. Variation of LM Exhaust Contamination with Time (Number of Particles/cm^3 versus Time in Seconds) for (a) $J = 10^9$, (b) $J = 10^{12}$	57
14	NO — Model I. Variation of LM Exhaust Contamination with Time (Number of Particles/cm^3 versus Time in Seconds) for (a) $J = 10^9$, (b) $J = 10^{12}$	58
15	O_2 — Model I. Variation of LM Exhaust Contamination with Time (Number of Particles/cm^3 versus Time in Seconds) for (a) $J = 10^9$, (b) $J = 10^{12}$	58
16	H_2O — Model II. Variation of LM Exhaust Contamination with Time (Log of Number of Particles/cm^3 versus Log of Time in Seconds) at 30 to 300 Meters from LM Touchdown for (a) No sticking, (b) Sticking	59

Figure		Page
17	H_2O — Model II. Variation of LM Exhaust Contamination with Time (Log of Number of Particles/cm^3 versus Log of Time in Seconds) at 2700 km from LM Touchdown for (a) No Sticking, (b) Sticking	59
18	H_2O — Model II. Variation of LM Exhaust Contamination with Time (Log of Number of Particles/cm^3 versus Log of Time in Seconds) at 5600 km from LM Touchdown for No Sticking	60
19	N_2 — Model II. Variation of LM Exhaust Contamination with Time (Log of Number of Particles/cm^3 versus Log of Time in Seconds) at 30 to 300 Meters from LM Touchdown for (a) No Sticking, (b) Sticking	60
20	N_2 — Model II. Variation of LM Exhaust Contamination with Time (Log of Number of Particles/cm^3 versus Log of Time in Seconds) at 2700 km from LM Touchdown for (a) No Sticking, (b) Sticking	61
21	N_2 — Model II. Variation of LM Exhaust Contamination with Time (Log of Number of Particles/cm^3 versus Log of Time in Seconds) at 5600 km from LM Touchdown for No Sticking	61
22	H_2 — Model II. Variation of LM Exhaust Contamination with Time (Log of Number of Particles/cm^3 versus Log of Time in Seconds) at 30 to 300 Meters from LM Touchdown for No Sticking	61

Figure		Page

23 H_2 — Model II. Variation of LM Exhaust Contamination with Time (Log of Number of Particles/cm^3 versus Log of Time in Seconds) at 2700 km from LM Touchdown for No Sticking 62

24 H_2 — Model II. Variation of LM Exhaust Contamination with Time (Log of Number of Particles/cm^3 versus Log of Time in Seconds) at 5600 km from LM Touchdown for No Sticking 62

25 CO — Model II. Variation of LM Exhaust Contamination with Time (Log of Number of Particles/cm^3 versus Log of Time in Seconds) at 30 to 300 Meters from LM Touchdown for No Sticking 62

26 CO — Model II. Variation of LM Exhaust Contamination with Time (Log of Number of Particles/cm^3 versus Log of Time in Seconds) at 2700 km from LM Touchdown for No Sticking 62

27 CO — Model II. Variation of LM Exhaust Contamination with Time (Log of Number of Particles/cm^3 versus Log of Time in Seconds) at 5600 km from LM Touchdown for No Sticking 63

Figure		Page
28	CO_2 — Model II. Variation of LM Exhaust Contamination with Time (Log of Number of Particles/cm^3 versus Log of Time in Seconds) at 30 to 300 Meters from LM Touchdown for No Sticking	63
29	CO_2 — Model II. Variation of LM Exhaust Contamination with Time (Log of Number of Particles/cm^3 versus Log of Time in Seconds) at 2700 km from LM Touchdown for No Sticking	63
30	CO_2 — Model II. Variation of LM Exhaust Contamination with Time (Log of Number of Particles/cm^3 versus Log of Time in Seconds) at 5600 km from LM Touchdown for No Sticking	63
31	H — Model II. Variation of LM Exhaust Contamination with Time (Log of Number of Particles/cm^3 versus Log of Time in Seconds) at 30 to 300 Meters from LM Touchdown for No Sticking	64
32	H — Model II. Variation of LM Exhaust Contamination with Time (Log of Number of Particles/cm^3 versus Log of Time in Seconds) at 2700 km from LM Touchdown for No Sticking .	64
33	H — Model II. Variation of LM Exhaust Contamination with Time (Log of Number of Particles/cm^3 versus Log of Time in Seconds) at 5600 km from LM Touchdown for No Sticking .	64

Figure		Page

34 OH — Model II. Variation of LM Exhaust Contamination with Time (Log of Number of Particles/cm^3 versus Log of Time in Seconds) at 30 to 300 Meters from LM Touchdown for (a) No Sticking, (b) Sticking 65

35 OH — Model II. Variation of LM Exhaust Contamination with Time (Log of Number of Particles/cm^3 versus Log of Time in Seconds) at 2700 km from LM Touchdown for (a) No Sticking, (b) Sticking 65

36 OH — Model II. Variation of LM Exhaust Contamination with Time (Log of Number of Particles/cm^3 versus Log of Time in Seconds) at 5600 km from LM Touchdown for No Sticking . 66

37 NO — Model II. Variation of LM Exhaust Contamination with Time (Log of Number of Particles/cm^3 versus Log of Time in Seconds) at 30 to 300 Meters from LM Touchdown for (a) No Sticking, (b) Sticking 66

38 NO — Model II. Variation of LM Exhaust Contamination with Time (Log of Number of Particles/cm^3 versus Log of Time in Seconds) at 2700 km from LM Touchdown for (a) No Sticking, (b) Sticking 67

39 NO — Model II. Variation of LM Exhaust Contamination with Time (Log of Number of Particles/cm^3 versus Log of Time in Seconds) at 5600 km from LM Touchdown for No Sticking 67

Figure		Page
40	O_2 — Model II. Variation of LM Exhaust Contamination with Time (Log of Number of Particles/cm^3 versus Log of Time in Seconds) at 30 to 300 Meters from LM Touchdown for (a) No Sticking, (b) Sticking	68
41	O_2 — Model II. Variation of LM Exhaust Contamination with Time (Log of Number of Particles/cm^3 versus Log of Time in Seconds) at 2700 km from LM Touchdown for (a) No Sticking, (b) Sticking	68
42	O_2 — Model II. Variation of LM Exhaust Contamination with Time (Log of Number of Particles/cm^3 versus Log of Time in Seconds) at 5600 km from LM Touchdown for No Sticking .	69
43	O — Model II. Variation of LM Exhaust Contamination with Time (Log of Number of Particles/cm^3 versus Log of Time in Seconds) at 30 to 300 Meters from LM Touchdown for (a) No Sticking, (b) Sticking	69
44	O — Model II. Variation of LM Exhaust Contamination with Time (Log of Number of Particles/cm^3 versus Log of Time in Seconds) at 2700 km from LM Touchdown for (a) No Sticking, (b) Sticking	70
45	O — Model II. Variation of LM Exhaust Contamination with Time (Log of Number of Particles/cm^3 versus Log of Time in Seconds) at 5600 km from LM Touchdown for No Sticking	70

Figure		Page

46 Comparison of Model I Densities (Scaled Down by a Factor of 1/10) with Model II Densities for CO. No Sticking 71

47 Comparison of the Model II Densities of H_2O for Three Values of φ when $\theta = 90°$. No Sticking 71

48 Comparison of Model II Densities of H_2O, H, O_2 for $\theta = .01°$ with $\theta = 90°$. No Sticking 72

49 Comparisons of the Variations with Time for Model II Densities of H_2O, CO_2, NO, O, H at $\theta = .01°$. No Sticking 72

50 Comparisons of Model II Densities of H_2O, O for the No Sticking with the Sticking Case at $\theta = .01°$ 73

51 Variation of Total Densities of Contaminants with Time at 30 to 300 Meters from LM Touchdown 73

I. INTRODUCTION

In this report, the variation of the tenuous lunar atmosphere with time and position is investigated as a function of the sources of lunar atmospheric gases that also vary with time and with position. As an example, the contamination of the lunar atmosphere by the Apollo mission rockets is calculated.

Variations in the lunar atmosphere may arise from variations of the (natural and artificial) sources of gas, or from changes in the environment. Changes in the atmosphere due to point sources of gas are herein considered as functions of time and position, with changes in the environmental parameters such as lunar surface temperature and the solar wind intensity and velocity introduced only on a steady-state basis.

To make the problem tractable, two models of lunar atmosphere variation have been adopted. The first model assumes that all quantities are independent of latitude and longitude on the moon, and finds a space-independent time variation of the atmospheric gases as a function of solar wind intensity and surface temperature. In the second model, point sources are introduced at arbitrary positions on the moon, and some of the environmental parameters have a simple dependence with position on the moon; an appropriate diffusion equation is solved to give the atmospheric species density as a function of position on the lunar surface, solar wind intensity, and time.

As an example of variations due to artificial sources of gas, manned and unmanned expeditions to the moon will introduce contaminant gases into the ambient lunar atmosphere. Dominant among these will be the exhaust gases from large, manned lunar landing vehicles. In particular, the Lunar Module (LM) will exhaust a

relatively large mass of gas in its descent to the lunar surface. These gases can produce significant variations in the rarefied natural atmosphere for appreciably long times. To interpret the measurements that will be made of the gases in the lunar atmosphere during and after the LM stay on the moon, estimates are made in this report of the contamination of the ambient lunar atmosphere by the exhaust gases. Adopting, as a source function for the atmospheric contaminants, the appropriate fraction of the space and time distribution of the LM gases striking the lunar surface, calculations have been made of atmosphere contamination by means of the two models introduced above.

In the following sections, the space-independent and space-dependent models (I and II, respectively) of atmospheric variation are formulated and the basic gas distribution equations are solved. This formulation holds for both natural and artificial sources, within the limitations of the two models. The atmospheric source and loss mechanisms are discussed, with particular attention to the contaminant gas species produced by the LM rocket exhaust hitting the moon's surface. Numerical results are then presented, for this particular case of lunar atmosphere variation due to the Apollo mission, in the form of graphs of the atmospheric contaminant distribution with position on the moon and time after initial ignition of the LM descent rockets. Finally the contamination implications are discussed.

During the LM stay-time, the contamination of the atmosphere is shown to be both appreciable and nonuniform in distribution, with the subsequent trend toward a uniform distribution proceeding at different rates for different exhaust gas species.

II. MODEL FORMULATION

A. Model I - Time Dependence Only

1. Assumptions

A simplified model is adopted as a first attempt at a theoretical treatment of the variations produced in the density of the tenuous lunar atmosphere by different source and loss mechanisms. In this model it is assumed that the particles of each gas species in the lunar atmosphere: 1) are contained in the volume, V, between the surface of the moon and a surface at scale height, h, defined below; 2) have a number density, n, that is uniform throughout V at a given time, t, so that n is a function only of the time and is independent of the space coordinates within the volume, V. Further, it is assumed that the natural sources and any artificially introduced sources are uniformly distributed over the lunar surface, from which they are emitted into the atmosphere at the temperature of the surface that is taken as constant. The atmosphere is assumed to be isothermal, and to have the same temperature, T, as the surface ($T = 300°K$ for all our calculations here).

Because the lunar atmosphere is extremely rarefied, it is assumed that the atmospheric gas particles do not collide with one another but only with the lunar surface and the incoming solar wind particles and solar photons.

For a source or sources of finite life, this model should give the asymptotic values of the atmospheric gas densities approached by more sophisticated space-dependent distribution models because the mean free path of the gas molecules is very large and uniform distributions are approached after long times.

2. Equations

If the total number of particles, N, of a given species of gas is contained in the volume, V, between the surface of the moon (of radius r_o) and a spherical surface at height h, then

$$N = nV ,$$

where n is the number density of the gas species in question and the "scale volume" is

$$V = \frac{4}{3}\pi \left[(r_o + h)^3 - r_o^3 \right] ,$$

while the "scale height" for a gas of particles of mass, m, is

$$h = \frac{kT}{mg} .$$

The number density, n, is taken as constant throughout the volume, V, and therefore it also represents the average number density at the surface. Then, in this simple model, n is time dependent only and its time rate of change is given by

$$\frac{dn}{dt} + An = \frac{1}{V} [B + C(t)] , \qquad (1)$$

where

An = the number of particles of a given species of gas lost per second from the atmosphere via processes such as collisions with solar wind particles and solar photons and thermal evaporation

B = the number of particles of a given gas species emitted per second into the atmosphere from the lunar surface due to:

a) neutralization and diffuse reflection of solar wind ions at the surface

b) actual steady-state sources in the lunar surface crust.

$C(t)$ = the number of particles of a given species of gas emitted per second from additional, time-dependent, sources on the lunar surface.

Assuming that the gases from the time-dependent sources are emitted from the lunar surface at a constant time rate and then stop, we let

$$C(t) = D_1 \cdot U(t) \ , \tag{2a}$$

where $U(t)$ is the step-function of time

$$U(t) = \begin{cases} 1, & 0 \leq t \leq \tau \\ 0, & t > \tau \end{cases} \ . \tag{2b}$$

τ is the total time interval during which this gas is being emitted, and

D_1 = number of particles of a given species of this gas emitted per second from the lunar surface over the time interval τ [see Eqs. (40) and (47) below].

3. Solutions

The solutions of Eq. (1) in the time intervals of Eq. (2b) are found by well-known integration techniques. If $n = n_o$ at $t = 0$, then

$$n(t)\ e^{At} = \frac{1}{V}\int_0^t [B + C(t)]\ e^{At}\ dt + n_o\ .$$

If $C(t)$ is defined by Eqs. (2), then

<u>for $t \leq \tau$:</u>

$$n(t) = \frac{B + D_1}{AV} + e^{-At}\left[n_o - \frac{B + D_1}{AV}\right]\ . \tag{3}$$

<u>For $t \geq \tau$:</u>

$$n(t) = \frac{B}{AV} + e^{-At}\left\{n_o - \frac{B - D_1(e^{A\tau} - 1)}{AV}\right\}\ . \tag{4}$$

It is clear from Eq. (4) that for times, t, very long compared to τ,

$$n(t) \xrightarrow[\substack{t \gg \tau \\ t \to \infty}]{} \frac{B}{AV}\ ,$$

which shows that in this simple theory there is no residual effect of the gas species from time-dependent sources (D_1) and the particle density attains an equilibrium value at sufficiently long times.

Furthermore, $B = 0$ for those gas species that emanate solely from time-dependent sources, D_1, and for times, t, less than or equal to τ, it is clear from Eq. (3) that

$$n(t) = \frac{D_1}{AV}\ (1 - e^{-At})\ , \qquad (t \leq \tau)$$

when $n_o = 0$. In addition, if the loss rate, A, for these gas species is small enough that $\tau \ll 1/A$, then for times, t, less than or equal to τ,

$$n(t) \simeq \frac{D_1 t}{V} . \tag{5}$$

Also, under these same assumptions that $B = 0$, $n_o = 0$, and $\tau \ll 1/A$, it is clear from Eq. (4) that for times, t, greater than τ,

$$n(t) \simeq \frac{D_1 \tau \, e^{-At}}{V} . \tag{6}$$

Thus, for those species that emanate solely from the time-dependent sources (D_1) and for which their loss rate is such that $\tau \ll 1/A$, the plot in Fig. 1 of Eqs. (5) and (6) shows their simple linear build-up and subsequent exponential decay.

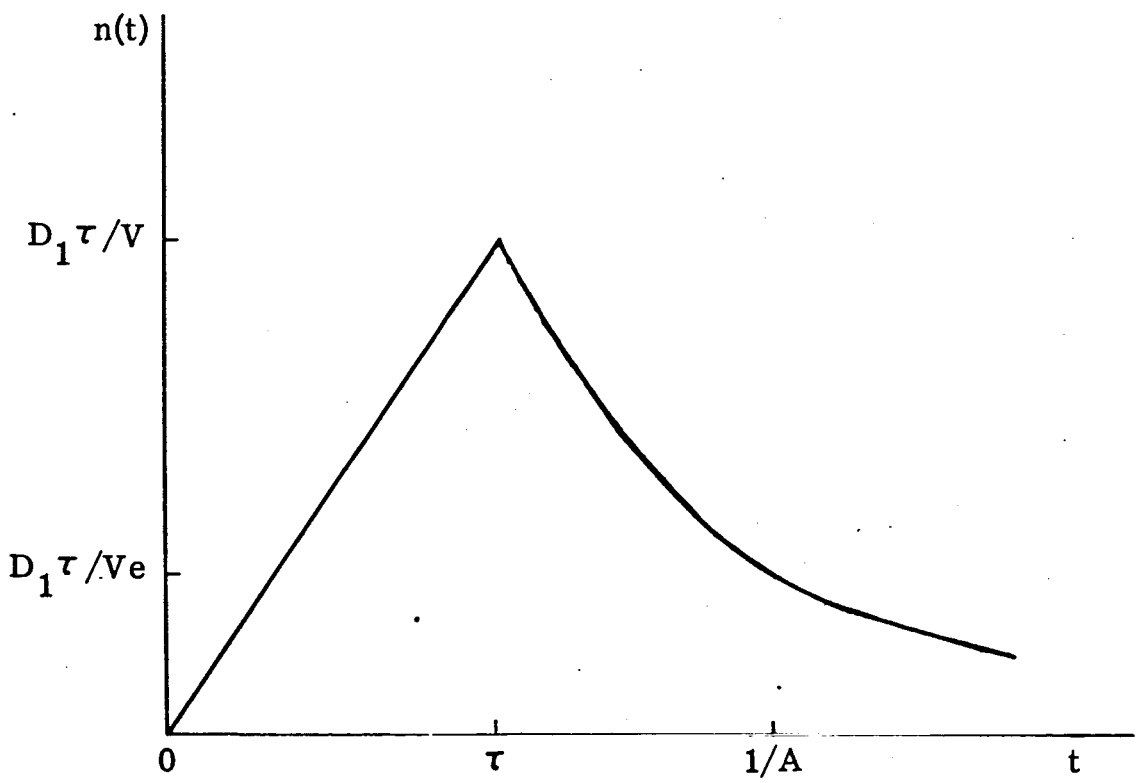

Fig. 1 Variation of the Particle Number Density with Time as Given by Equations (5) and (6)

Furthermore, it is seen from Eq. (6) that when $\tau < t \ll 1/A$, the particle density is approximately independent of t:

$$n(t) \simeq D_1\tau/V \quad .$$

[From Eqs. (40) or (47) below it is seen that $n(t)$ is also independent of τ in this time interval.]

These general features are evident in the Figs. 5 through 15 of Section IV.

B. Model II - Space and Time Dependence

1. Assumptions

In this model an attempt is made to obtain the spatial distribution of gases in the lunar atmosphere as well as their temporal fluctuations. From an initial distribution of gas sources on the lunar surface, the gas particles undergo a three dimensional diffusion into the thin lunar atmosphere. The gas particles move in ballistic trajectories between collisions with the surface. Collisions between gas particles may be neglected because the gas-gas mean free path is large compared to the gas-surface mean free path. A three dimensional diffusion process is mathematically complicated because of the presence of gravitational forces and intricate particle trajectories between collisions, so we consider instead a reasonable two dimensional model of the diffusion. In this, the gas particles are assumed to diffuse only along (parallel to) the lunar surface from constant temperature sources on the surface. The diffusing molecules suffer losses due to interactions with the solar wind particles and solar ultraviolet photons, thermal evaporation, and also due to adsorption on the lunar surface. Also the particle density is assumed uniform in the vertical column of scale height, h, above each point on the surface. For sources of finite life, as the diffusing particles approach a uniform distribution over the lunar surface, the atmospheric densities should approach those of Model I.

2. Equations

Choosing the diffusion coefficient D as a constant for each species of exhaust gas, the diffusion equation for the particle density n (particles/cm^3) is

$$\frac{\partial n}{\partial t} = D\nabla^2 n + q(r,\theta,\varphi,t) + Kn \ , \tag{7}$$

where q is a source term (cm^{-3}sec^{-1}) that is not explicitly dependent on the number density, n, at each point (r,θ,φ), and K is the time-rate coefficient (sec^{-1}) of the loss term that is explicitly n dependent. The constant diffusion coefficient D is given by

$$D = \frac{1}{3}\lambda v \ ,$$

where

λ = mean free path of a gas particle

v = velocity of reemission of a gas particle from the lunar surface.

The three dimensional diffusion problem, Eq. (7), is now replaced by a two dimensional model of diffusion on a spherical surface. In this, the molecules are assumed to diffuse only along the lunar surface, $r = r_o$. They suffer losses of $K'n'$ particles per cm^2 per sec, where n' is the surface particle density in units of cm^{-2}, due to interactions with solar wind particles, solar ultraviolet photons, thermal evaporation at the top of the atmosphere, and also due to adsorption when the diffusing molecules strike the surface. It is assumed that the surface sources of the diffusing gas molecules are represented by the function $q'(\theta,\varphi,t)$ in units of cm^{-2}sec^{-1}, where $q'(\theta,\varphi,t)$ is not explicitly dependent on the particle density n' at each point

(θ,φ) on the surface. Finally, choosing the diffusion coefficient D' as a constant for each species of gas, we obtain the two dimensional diffusion equation by analogy with Eq. (7):

$$\frac{\partial n'}{\partial t} = D'\nabla_2^2 n' + q'(\theta,\varphi,t) + K'n' , \tag{8}$$

where ∇_2^2 is the two dimensional Laplacian operator on a spherical surface

$$\nabla_2^2 = \frac{1}{r_o^2}\left\{\frac{1}{\sin\theta}\frac{\partial}{\partial\theta}\left(\sin\theta\frac{\partial}{\partial\theta}\right) + \frac{1}{\sin^2\theta}\frac{\partial^2}{\partial\varphi^2}\right\} .$$

The constant diffusion coefficient D' is given by

$$D' = \frac{1}{3}\lambda' v ,$$

where

λ' = a gas particle's mean free path along the lunar surface, and

v = the velocity of reemission of a gas particle from the lunar surface.

The solution $n'(r_o,\theta,\varphi;\ t)$ of Eq. (8), under the proper initial and boundary conditions, together with the assumption that the particle density is uniform in the vertical column of scale height h above each point on the surface will yield the volume number density $n(r,\theta,\varphi;\ t) = n'(r_o,\theta,\varphi;\ t)/h$ in cm^{-3}.

The initial condition on Eq. (8) is

$$n'(r_o,\theta,\varphi;\ 0) = n_o' , \tag{9}$$

where n_o' = surface number density at time $t = 0$ due to the ambient atmosphere such that

$$n_o' = \int_{r_o}^{\infty} n_o(r,\theta,\varphi;\ 0)\ dr\ .$$

Taking the origin of the spherical polar coordinates (r,θ,φ) at the center of the moon and a point L on the surface as the pole, the boundary conditions on Eq. (8) are:

$$\begin{aligned} n'(\theta,\varphi;\ t) &= n'(2\pi + \theta,\varphi;\ t) \\ n'(\theta,\varphi;\ t) &= n'(\theta,\varphi + 2\pi;\ t) \end{aligned} \tag{10}$$

3. Solutions

To solve Eq. (8), we let $\mu = \cos\theta$ and take n', q' as φ independent; then

$$n'(\theta,\varphi;\ t) = n'(\mu,t)\ ,$$

$$q'(\theta,\varphi;\ t) = q'(\mu,t)\ ,$$

and Eq. (8) takes the form

$$\frac{\partial n'(\mu,t)}{\partial t} = \frac{D'}{r_o^2}\frac{\partial}{\partial\mu}\left[(1-\mu^2)\frac{\partial n'}{\partial\mu}\right] + q'(\mu,t) + K'n'\ . \tag{11}$$

Integrating this equation over t from 0 to ∞ by the Laplace transform technique, we obtain

$$p\overline{n'}(\mu,p) - n'(\mu,0) = \frac{D'}{r_o^2}\frac{d}{d\mu}\left[(1-\mu^2)\frac{d\overline{n'}}{d\mu}\right] + \overline{q'}(\mu,p) + K'\overline{n'}\ ,$$

where the Laplace transform $\overline{n'}(\mu,p)$ of $n'(\mu,t)$ is defined by

$$\overline{n'}(\mu,p) = \int_0^\infty e^{-pt}\, n'(\mu,t)\, dt \;;$$

and upon regrouping the terms

$$-\frac{d}{d\mu}\left[(1-\mu^2)\frac{d\overline{n'}}{d\mu}\right] + \frac{r_o^2}{D'}(p - K')\overline{n'} = \frac{r_o^2}{D'}\left[\overline{q'}(\mu,p) + n'(\mu,0)\right] . \qquad (12)$$

The first term on the left side of Eq. (12) contains the Legendre operator Ω (Ref. 1), with the eigenvalues $\ell(\ell+1)$; $\ell = 0,1,2,\ldots$

$$\Omega\overline{n'} = -\frac{d}{d\mu}\left[(1-\mu^2)\frac{d\overline{n'}}{d\mu}\right] = \ell(\ell+1)\overline{n'} , \qquad (13)$$

Thus, Eq. (12) can be written in the form

$$[\Omega - \omega_o(p)]\,\overline{n'} = F(\mu,p) , \qquad (14)$$

where

$$\omega_o(p) = -\frac{r_o^2}{D'}(p - K') ,$$

and (15)

$$F(\mu,p) = \frac{r_o^2}{D'}\left[\overline{q'}(\mu,p) + n'(\mu,0)\right] .$$

The normalized eigenfunction solutions to Eq. (13) are (Ref. 1)

$$\Theta_\ell(\mu) = \left(\frac{2\ell+1}{2}\right)^{\frac{1}{2}} P_\ell(\mu) ,$$

where $P_\ell(\mu)$ are the Legendre polynomials and the orthonormality and closure conditions on the Θ_ℓ are, respectively,

$$\int_{-1}^{+1} \Theta_\ell(\mu)\Theta_{\ell'}(\mu)\ d\mu = \delta_{\ell\ell'}$$

$$\sum_{\ell=0}^{\infty} \Theta_\ell(\mu)\Theta_\ell(\mu') = \delta(\mu - \mu') \ .$$

It then follows that the solution of Eq. (14) is given in terms of a Green's function G_{ω_o} by:

$$\overline{n'}(\mu,p) = \int_{-1}^{+1} G_{\omega_o}(\mu,\mu')F(\mu',p)\ d\mu' \ , \tag{16}$$

where

$$G_{\omega_o}(\mu,\mu') = \sum_{\ell=0}^{\infty} \frac{\Theta_\ell(\mu)\Theta_\ell(\mu')}{\omega - \omega_o} \ , \tag{17}$$

and

$$\omega = \ell(\ell + 1) \ .$$

Using Eqs.(15), the explicit dependence on ℓ and p of the Green's function in Eq. (17) and the solution $\overline{n'}(\mu,P)$ are obtained:

$$G_\ell(\mu,\mu',p) = \frac{D'}{r_o^2} \sum_{\ell=0}^{\infty} \frac{\Theta_\ell(\mu)\Theta_\ell(\mu')}{p - K' + \frac{D'}{r_o^2}\ \ell(\ell + 1)} \ , \tag{18}$$

$$\overline{n'}(\mu,p) = \sum_{\ell=0}^{\infty} \frac{\Theta_\ell(\mu)}{p + a_\ell} \int_{-1}^{+1} \Theta_\ell(\mu') \left[\overline{q'}(\mu',p) + n'(\mu',0)\right] d\mu' , \tag{19}$$

where

$$a_\ell = - K' + \frac{D'}{r_o^2} \ell(\ell + 1) . \tag{20}$$

Taking the inverse Laplace transform of Eq. (19),

$$n'(\mu,t) = \frac{1}{2\pi i} \int_{-i\infty+\epsilon}^{i\infty+\epsilon} \overline{n'}(\mu,p)\, e^{pt}\, dp \qquad \text{Re } t > 0 ,$$

choosing the path of integration in the p-plane as indicated in Fig. 2,

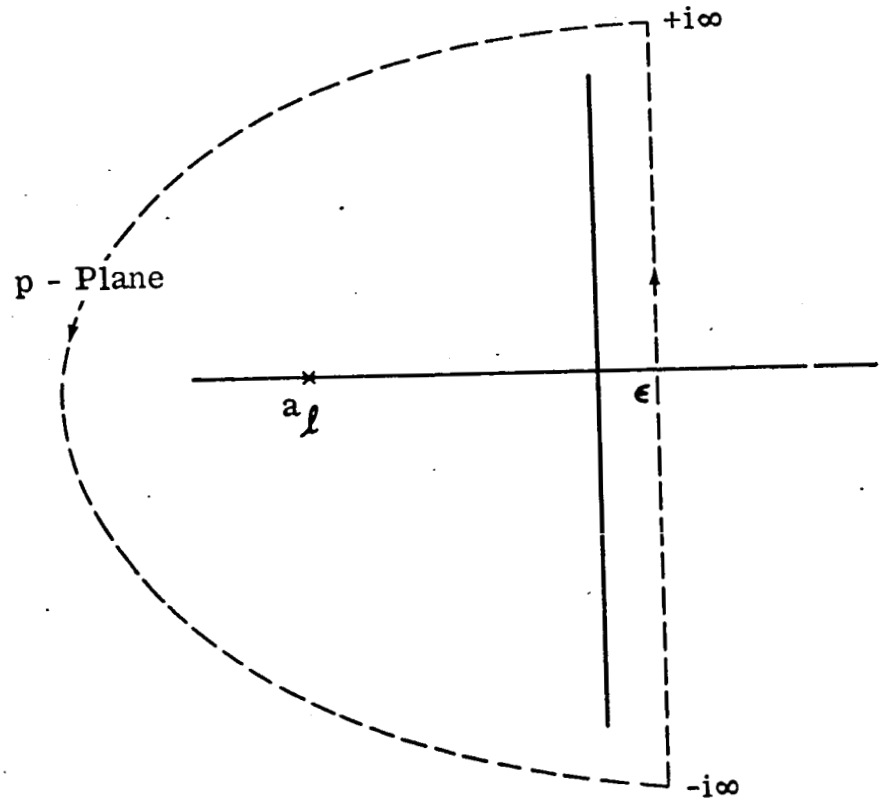

Fig. 2 Path of Integration in the p-plane

and letting $\epsilon \to 0$, we obtain

$$n'(\mu,t) = \frac{1}{2\pi i}\int_{-i\infty}^{+i\infty} \overline{n'}(\mu,p)\, e^{pt}\, dp$$

$$= \frac{1}{2\pi i}\sum_{\ell=0}^{\infty} \Theta_\ell(\mu) \int_{-1}^{+1} \Theta_\ell(\mu') \left\{ \int_{-i\infty}^{+i\infty} \frac{\overline{q'}(\mu',p)}{p + a_\ell}\, e^{pt}\, dp \right.$$

$$\left. + \int_{-i\infty}^{+i\infty} \frac{n'(\mu',0)}{p + a_\ell}\, e^{pt}\, dp \right\} d\mu' \;;$$

or

$$n'(\mu,t) = \sum_{\ell=0}^{\infty} \Theta_\ell(\mu) \int_{-1}^{+1} \Theta_\ell(\mu') \left[Q_\ell(\mu',t) + R_\ell(\mu',t) \right] d\mu' \;, \tag{21}$$

where

$$Q_\ell(\mu',t) = \frac{1}{2\pi i}\int_{-i\infty}^{+i\infty} \frac{\overline{q'}(\mu',p)}{p + a_\ell}\, e^{pt}\, dp \tag{22}$$

$$R_\ell(\mu',t) = \frac{1}{2\pi i}\int_{-i\infty}^{+i\infty} \frac{n'(\mu',0)}{p + a_\ell}\, e^{pt}\, dp = n'(\mu',0)\, e^{-a_\ell t} \;. \tag{23}$$

Then, the solution of Eq. (11) in analytical form is

$$n'(\mu,t) = \sum_{\ell=0}^{\infty} \Theta_\ell(\mu)\left[S_\ell(t) + T_\ell(t)\right] , \tag{24}$$

where

$$S_\ell(t) = \int_{-1}^{+1} \Theta_\ell(\mu')Q_\ell(\mu',t)\, d\mu' , \tag{25a}$$

and

$$T_\ell(t) = e^{-a_\ell t} \int_{-1}^{+1} \Theta_\ell(\mu')n'(\mu',0)\, d\mu' . \tag{25b}$$

To obtain an explicit expression for the solution, Eq. (24), we must now assume explicit functional forms for $q'(\mu,t)$ and $n'(\mu,0)$.

Let us start by assuming that the space and time parts of the source function can be separated and written as

$$q'(\mu,t) = q'_\mu(\mu)q'_t(t) . \tag{26}$$

The Laplace transform of Eq. (26) is

$$\overline{q'}(\mu,p) = q'_\mu(\mu)\overline{q'_t}(p) .$$

Substitution of this equation into Eq. (22) yields

$$Q_\ell(\mu',t) = \frac{1}{2\pi i}\, q'_\mu(\mu') \int_{-i\infty}^{+i\infty} \frac{\overline{q'_t}(p)\, e^{pt}}{p + a_\ell}\, dp \tag{27a}$$

Now, assuming that $\overline{q'_t}(p)$ has no poles in p, and applying Cauchy's theorem we obtain

$$Q_\ell(\mu',t) = q'_\mu(\mu')\, \overline{q'_t}(-a_\ell)\, e^{-a_\ell t} . \tag{27b}$$

Using Eq. (27b), Eq. (25a) becomes

$$S_\ell(t) = \overline{q'_t}(-a_\ell)\, e^{-a_\ell t} \int_{-1}^{+1} \Theta_\ell(\mu')\, q'_\mu(\mu')\, d\mu' \tag{28}$$

We now take the source function $q'(\mu,t)$ [Eqs. (11) and (26)] to be a point source at the pole $\theta_i = 0$ on the lunar surface. We assume that it is "turned-on" briefly at time t_k and proceed to find the surface distribution $n'(\mu,t)$, at times $t > t_k$, of the gas molecules that diffuse from this point source. From the functional form of this distribution, we will generalize later to the distribution due to a point source at <u>any</u> point (θ_i,φ_j) on the lunar surface. Finally, we will sum over the contributions from all the point sources to obtain the surface distribution $n'(\mu,t)$. Therefore, we start by taking a point source at the pole $(\theta_i = 0)$

$$q'_\mu(\mu) = q_o\,\delta(\mu - 1) \tag{29a}$$

at time $t = t_k$

$$q_t'(t) = \delta(t - t_k) \ , \tag{29b}$$

and note that $q_\mu'(\mu)$ and $q_t'(t)$ have the dimensions cm^{-2} and sec^{-1}, respectively. Furthermore, we assume that the surface distribution of gas molecules is zero before the source is "turned-on" at $t = t_k$. In particular, at $t = 0$,

$$n'(\mu,0) = 0 \tag{29c}$$

It follows from Eq. (29b) that

$$\overline{q_t'}(p) = e^{-pt_k} \ . \tag{30}$$

Using Eqs. (30) and (29a), we obtain Eq. (28) in the form

$$S_\ell(t) = q_o \, e^{-a_\ell(t-t_k)} \int_{-1}^{+1} \Theta_\ell(\mu')\delta(\mu' - 1) \, d\mu' \ . \tag{31}$$

Thus,

$$S_\ell(t) = q_o \Theta_\ell(1) \, e^{-a_\ell(t-t_k)}$$

$$= q_o \sqrt{\frac{2\ell + 1}{2}} \, e^{-a_\ell(t-t_k)} \ . \tag{32}$$

Also, the substitution of Eq. (29c) into Eq. (25b) yields

$$T_\ell(t) = 0 \ . \tag{33}$$

Recalling that the solutions for $S_\ell(t)$ and $T_\ell(t)$ given in Eqs. (32) and (33), respectively, are for a point source at the pole $(\theta_i = 0)$ on the lunar surface, the substitution of these into Eq. (24) will give the surface density $n'(\mu,t)$ of the gas diffusing from this point at times $t > t_k$. Therefore, for $t > t_k$,

$$n'(\mu,t) = q_o \sum_{\ell=0}^{\infty} \sqrt{\frac{2\ell+1}{2}}\, \Theta_\ell(\mu)\, e^{-\left[|K'| + \frac{D'}{r_o^2}\ell(\ell+1)\right](t-t_k)} \tag{34a}$$

and for $t \leq t_k$,

$$n'(\mu,t) = 0 \ , \tag{34b}$$

where we have used Eq. (20) and have taken cognizance of the fact that K' is a negative quantity since it is the loss rate of the diffusing particles.

Introducing the step function

$$U'(t - t_k) = 0 \quad \text{for} \quad t \leq t_k$$
$$= 1 \quad \text{for} \quad t > t_k \ ,$$

Eqs. (34) can be combined into one equation for all $t \geq 0$:

$$n'(\mu,t) = q_o \sum_{\ell=0}^{\infty} \sqrt{\frac{2\ell+1}{2}}\, \Theta_\ell(\mu)\, e^{-\left[|K'| + \frac{D'}{r_o^2}\ell(\ell+1)\right](t-t_k)}\, U'(t - t_k) \ , \quad \theta_i = 0 \tag{35}$$

Generalizing from this result, it is clear that the contribution to the surface density at an observation point $P(\theta,\varphi)$ from a point source of strength (in cm^{-2}) q_{oijk} at $P'(\theta_i,\varphi_j)$ depends only on the angle α between P and P' (cf. Fig. 3 below) and the time interval $(t - t_k)$.

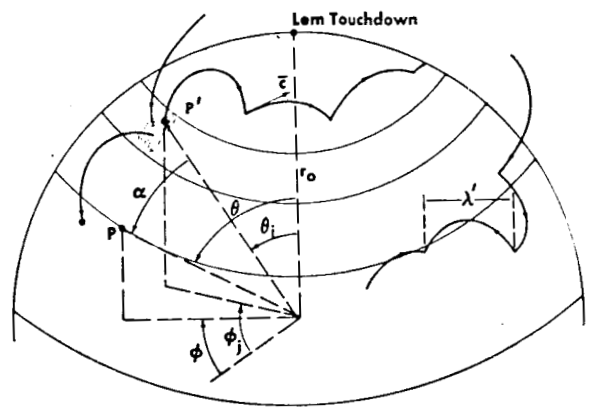

Fig. 3 Lunar Coordinate System for Model II

Therefore,

$$n'_{ijk}(\theta,\varphi,t) = q_{oijk} \sum_{\ell=0}^{\infty} \sqrt{\frac{2\ell+1}{2}}\, \Theta_\ell(\cos\alpha)$$

$$e^{-\left[|K'| + \frac{D'}{r_o^2}\ell(\ell+1)\right](t-t_k)} U'(t - t_k) , \qquad (36)$$

where q_{oijk} is defined in Eq. (41c) below, and

$$\cos \alpha = \cos \theta \cos \theta_i + \sin \theta \sin \theta_i \cos (\varphi - \varphi_j) .$$

The total surface density at a point $P(\theta,\varphi)$ at time $t > t_k$ of a given species of diffusing gas is the sum over all the point source contributions (36):

$$n'(\theta,\varphi,t) = \sum_{i,j,k} n'_{ijk}(\theta,\varphi,t) . \tag{37}$$

It should be made clear that Eq. (37) is applicable to all points, P, that are not source points and are at least several mean free path lengths λ' (Fig. 3) distant from a point source so that the diffusion theory is applicable.

If one makes the assumption that the distribution is the same throughout the scale height, h, above the surface point (θ,φ) as it is at this surface point, then the volume density $n(r,\theta,\varphi;\ t)$ of a given species of diffusing gas is obtained from Eq. (37) by

$$n(r,\theta,\varphi;\ t) = \frac{n'(r = r_o,\ \theta,\varphi;\ t)}{h} \tag{38}$$

in cm^{-3} when n' is in cm^{-2} and h is in cm.

III. ATMOSPHERIC SOURCE AND LOSS MECHANISMS

A. Source Mechanisms

1. Discussion

A number of natural source mechanisms have been proposed by various authors (Refs. 2-9) for the gases in the tenuous lunar atmosphere. They fall into two main categories. In the first are the sources assumed in the lunar surface crust itself, while in the second category are the influx of ions from the sun. The model chosen for the natural lunar atmosphere in this report is that of Hinton and Taeusch (Ref. 2)

In addition to the natural sources, manned and unmanned expeditions to the moon will introduce artificial or contaminant sources into the natural lunar environment. Major among these will be the exhaust gases from large, manned lunar landing vehicles. In particular, the Lunar Module (LM) will exhaust a relatively large amount of gas in its descent to the lunar surface. Because a knowledge of the distribution of rocket exhaust contaminants is of particular importance to the lunar-surface-and-atmosphere sample collection and analysis phases of the LM mission, and since this source can be represented in a suitable way for treatment by our Models I and II, we consider this case as an example of variations in the natural lunar atmosphere.

2. Model I

In the differential equation [cf. Sec. II, Eq. (1)] for this model we have introduced two source terms, B and $C(t)$. We now let B represent the natural sources of the lunar atmosphere and $C(t)$ represent the LM exhaust source. Following Hinton and Taeusch (Ref. 2), we have expressed B in the form

$$B = XJ\pi r_o^2 + J_s 4\pi r_o^2 \,, \tag{39}$$

and we have chosen $n_o = B/AV$ in Eqs. (3) and (4). The first term in Eq. (39) represents the number of particles of a given gas species emitted per second into the lunar atmosphere due to the neutralization and diffuse reflection of solar wind ions at the lunar surface. The solar wind is assumed to have a uniform flux of J positive ions per cm^2 per second at each point on the sunlit side of the lunar surface. Then the effective capture cross section of the moon for these ions is πr_o^2, where r_o is the lunar radius. They strike the moon, are neutralized, and reemitted as neutral gas atoms with a Maxwellian distribution of velocities at the temperature of the surface. This is pictured as process B_1 in Fig. 4. X represents the fraction of positive ions of a

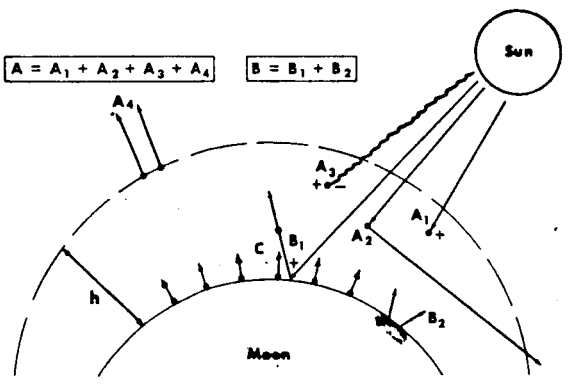

Fig. 4 Pictorialization of the Lunar Atmospheric Source and Loss Mechanisms

particular species in the solar wind. Since the solar wind is composed chiefly of protons, alpha particles, and electrons, following Hinton and Taeusch (Ref. 2), who in turn adapted their estimates from Aller's work (Ref. 10), we have taken $X = 0.86$ for H and $X = 0$ for all the other species in the LM exhaust (cf. Table 1). This process thus becomes an important source of H atoms in the natural lunar atmosphere.

The second term in Eq. (39) represents the number of particles of a given gas species emitted per second into the lunar atmosphere due to the flux, J_s, of such gas particles from sources in the lunar surface crust. This is pictured as process B_2 in Fig. 4. At present any estimates of these natural surface sources must be considered to be quite speculative. Hinton and Taeusch (Ref. 2) estimate that $J_s = 1.5 \times 10^5$ molecules per cm^2 per sec is the average value for water vapor flux for the entire lunar surface due to the evaporation of ice, which possibly has been retained on those portions of the lunar surface that are permanently shaded from the sun. For all the other gas species that appear in the LM exhaust (Table 1), we have taken $J_s = 0$, although the literature does contain estimates of J_s for some of these species. For example, Vestine (Ref. 8) gives estimates of J_s for CO_2 based on the assumptions that the composition of the moon is similar to the earth' crust and mantle, and that its yield per year is proportional to the surface area. He gives the seemingly high value of $J_s = 10^{10}$ molecules/cm^2sec.

Table 1

VALUES OF THE INPUT PARAMETERS FOR MODELS I AND II

Exhaust Species (S)	Y	β*	$\bar{\gamma}$	$\sigma_{e\ell}(H^+,S) \times 10^{16}(cm^2)$	$\sigma'_{e\ell}(H^+,S) \times 10^{16}(cm^2)$	$\sigma_{ex}(H^+,S) \times 10^{15}(cm^2)$	$\sigma_{ex}(He^{++},S) \times 10^{15}(cm^2)$	$\Sigma\sigma\Phi_o \times 10^6(sec^{-1})$	$A \times 10^5(sec^{-1})$** $J = 10^9$	$A \times 10^5(sec^{-1})$** $J = 10^{12}$
H_2O	.36	.5	.5	5.8	5.8	2.0	2.0	19.0	1.01	65.5
N_2	.32	.5	.5	11.3	0.65	1.0	0.4	5.0	0.296	46.4
H_2	.13	1.0	1.0	5.8	5.8	0.5	0.1	1.0	14.3	116.6
CO	.096	.5	.5	11.2	0.65	2.7	2.7	5.0	0.383	132.9
CO_2	.037	.5	.5	16.8	0.45	1.0	1.0	10.0	0.55	50.9
H	.019	1.0	1.0	4.5	4.5	2.0	0.03	0.45	14.6	231.8
OH	.016	.5	.5	3.1	3.1	1.0	1.0	5.0	0.283	33.1
NO	.0024	.5	.5	11.1	0.55	1.0	1.0	5.0	0.30	50.4
O_2	.0015	.5	.5	10.3	0.45	1.0	0.7	5.0	0.298	48.2
O	.0014	.5	.5	6.9	6.9	0.5	0.4	1.0	0.0794	29.4

*These values of β are for Model I only.

**These values of A are for the listed values of β.

It should be stressed that the aim of our calculations is to find the contributions made to the lunar atmosphere by the LM exhaust gases, which are independent of the actual composition of the lunar atmosphere.

The major species of exhaust gases emanating from the descent engine of the LM are listed in Table 1. In this simple Model I we assume that a total mass, M, of exhaust gas strikes the lunar surface (spreads uniformly), accommodates to the surface temperature and then is reemitted at a uniform rate in the time τ seconds. This is pictured as process C in Fig. 4. Thus, the atmospheric source term C(t) for the LM exhaust gases is given by Eqs. (2) with D_1 defined by the equation

$$D_1 = \frac{N_A Y M}{W\tau} , \tag{40}$$

where

Y = mole fraction of a given species of gas in the exhaust,

M = total mass of exhaust gas in grams, arbitrarily chosen as 10^7 grams,

N_A = Avogadro's number,

W = molecular weight of the given species of gas.

The mole fractions (Y) of the major species of gases in the exhaust of the LM descent engine are listed in Table 1.

In our calculations we have chosen the values 100 seconds and 1000 seconds for τ as reasonable estimates.

3. Model II

In this model we have taken the atmospheric sources to be point sources q_{oijk} [cf. Sec. II.3, Eq. (36)] distributed over the lunar surface. In our calculations using this model we have ignored the natural sources and treated as atmospheric sources only the LM descent exhaust distributed on the lunar surface. The initial spatial distribution of the LM exhaust gas as it impinges on the lunar surface is taken as known input from far-field gas dynamics calculations (cf. Sec. IV A of Ref. 11). These calculations yield the total mass per unit area, $m(\theta_i, \varphi_j)$ (in slugs/ft^2), of LM exhaust gas that impinges on the lunar surface at the point (θ_i, φ_j) for a given LM descent trajectory.

Assuming that a fraction, f_1, of these fast particles of a given species stick to the lunar surface for periods that are long compared to the observation time t, then the number, n_{ij}, of molecules of this exhaust gas specie that are emitted per cm^2 is given by

$$n_{ij} = \frac{32.17 \times 10^3}{2.205(30.48)^2} \frac{N_A Y m(\theta_i, \varphi_j)}{W} (1 - f_1) \tag{41a}$$

where the parameters N_A, Y, W were defined in Section III.A.2 above and the numerical factor completes the conversion from slugs/ft^2 to molecules/cm^2. We have divided the lunar region over which the exhaust is distributed into small areas, $r_o \sin \theta_i \Delta\theta_i \Delta\varphi_j$, and assumed each species of exhaust gas is reemitted at a time t_k from each area element as a point source q_{oijk} located at its center (θ_i, φ_j).

To determine the source strength, q_{oijk}, equate the total molecules emitted by this small area as obtained from Eq. (41a) to those as given by using a point source

$$q(\theta,\varphi,t) = q_{oijk}\delta(\mu - \mu_i)\delta(\varphi - \varphi_j)\delta(t - t_k) \ , \tag{41b}$$

similar to that in Eqs. (26) and (29), but at a general point (θ_i,φ_j) rather than at the pole. Therefore,

$$n_{ij}r_o^2 \sin\theta_i\Delta\theta_i\Delta\theta_j = \int_0^t\int_{\Delta\varphi_j}\int_{\Delta\theta_i} q_{oijk}\delta(\mu - \mu_i)\delta(\varphi - \varphi_j)\delta(t - t_k)r_o^2 \, d\mu d\varphi dt$$

so that the source strength in molecules per cm^2 is

$$q_{oijk} = n_{ij} \sin\theta_i\Delta\theta_i\Delta\varphi_j$$

$$= \frac{32.17 \times 10^3}{2.205 \times (30.48)^2} \frac{N_A Ym(\theta_i,\varphi_j)}{W} (1 - f_1)\sin\theta_i\Delta\theta_i\Delta\varphi_j \tag{41c}$$

In the present calculations, we used the $m(\theta_i,\varphi_j)$ calculated (Ref. 11) for a LM trajectory that yielded a uniform distribution with respect to φ about the plane $\varphi_j = 0$. It was found that $m(\theta_i,\varphi_j) \approx 0$ for $\theta_i > 10°$ when the LM touchdown point is chosen as the pole of the spherical coordinate system and the origin is chosen at center of the moon (Fig. 3).

B. Loss Mechanisms

1. Discussion

Gas particles can be lost from an atmosphere by a number of processes. They can be lost by interactions with other atmospheric

gas particles, solar wind ions, solar photons, the lunar surface, and also by thermal evaporation (Jean's escape mechanism) from the top of the atmosphere.

In the tenuous lunar atmosphere [$\lesssim 10^6$ atoms/cm^3 is estimated by Elsmore (Ref. 12)] the mean-free-path between collisions is so large that we can consider collisions between the atmospheric gas particles to be negligible as a loss mechanism.

The solar wind total positive ion flux J in ions/cm^{2}sec is known to vary with solar activity, so that the flux XJ of a positive ion species of relative amount X in the solar wind will vary with time. Although we have used two values (10^9 and 10^{12} ions/cm^{2}sec) of J in our calculations of the atmospheric gas densities, we have assumed a constant value of 500 km/sec for the stream velocity. At this velocity the energies of the protons and alpha particles, which form the major* positive ion constituents of the solar wind, are such (of the order of 1 keV) that their important interactions with the atmospheric gas particles are elastic collisions and charge exchange collisions. These are pictured as processes A_2 and A_1, respectively, in Fig. 4. Estimates (with order of magnitude accuracy) of the cross sections $\sigma_{e\ell}$ (cf. discussion Sec. III.B.2 below) and σ_{ex} (chief source was Ref. 15) for these processes are listed in Table 1. The cross sections are much smaller for these collision processes when 500 km/sec electrons ($E \sim 1$ ev) are incident upon the atmospheric gases. Therefore, we have neglected electrons interacting with the atmospheric gases as an important loss mechanism.

---

*Following Hinton and Taeusch (Ref. 2) we have chosen $X = .86$ for H^+ and $X = .14$ for He^{++}.

Solar photons in the ultraviolet region of the spectrum can ionize and dissociate the atmospheric gases. These processes are pictured as A_3 in Fig. 4. Using Hinterreger's estimates (Ref. 13) of the solar photon flux Φ_o, together with estimates of photoionization and photodissociation cross sections, we have listed in Table 1 the combined loss rates $\Sigma\sigma\Phi_o$ due to photoionization and photodissociation of the gas species in the LM exhaust. It should be noted that while photoionization cross sections are available from the literature, photodissociation cross sections are not. We estimated these from the total photoabsorption cross sections that are available in the literature (chief source was Ref. 16)

To calculate the thermal evaporation we assume the lunar atmosphere is collisionless, isothermal at the temperature, T, of the lunar surface, of volume, V, and scale height, h, with the lunar surface as its base. Then, the rate of evaporation from the top of the atmosphere of the high velocity particles, which form the tail of the Maxwellian distribution of particle velocities in this atmosphere, is given by Jean's formula (Ref. 14) in sec^{-1}

$$\alpha = \frac{4\pi r^2}{V} \frac{\bar{c}}{4} e^{-r/h} \left(1 + \frac{r}{h}\right) , \tag{42}$$

where the mean thermal speed is

$$\bar{c} = \sqrt{\frac{8kT}{\pi m}} , \tag{43}$$

$$r = r_o + h ,$$

and m is the mass of a gas particle. This loss mechanism is pictured as A_4 in Fig. 4. In a first approximation we have chosen $r = r_o$.

The losses due to the interactions between the gas particles and the lunar surface are discussed below under Models I and II.

2. Model I

The loss rate (in sec^{-1}) for the mechanisms discussed above (Sec. III.B.1) are mathematically represented in this model by the quantity A in Eq. (1). Adopting the Hinton and Taeusch (Ref. 2) notation we write this in the form

$$A = \beta \left\{ J \left(\bar{\gamma} \sigma'_{e\ell} + \sum X\sigma_1 \right) + \sum \sigma\Phi_o + \frac{\pi r_o^2}{\beta V} \bar{c}\, e^{-r_o/h} \left(1 + \frac{r_o}{h} \right) \right\} . \qquad (44)$$

The first term of this equation represents the rate at which an atmospheric particle is lost as the result of an elastic collision with a solar wind ion. J is again the total positive ion flux in the solar wind per cm^2 per sec. As a first approximation we have ignored the difference between protons and alpha particles for the elastic scattering of the atmospheric particles and have considered the cross sections $\sigma'_{e\ell}$ for scattering through all angles greater than a minimum angle, so that the atmospheric particle gains at least enough energy in the process to enable it to escape. For the heavier atmospheric particles (N_2, CO, CO_2, NO, O_2) listed in Table 1 we have estimated $\sigma'_{e\ell}$ by interpolation from those $\sigma'_{e\ell}$ calculated by Hinton and Taeusch (Ref. 2) for Ar, Kr, and Xe using the Thomas-Fermi atomic model. For the lighter particles (H, H_2, O, OH, H_2O) in Table 1, where the Thomas-Fermi model presumably does not apply, we have used the gas kinetic cross sections $\sigma_{e\ell}$ (Refs. 2 and 14) and assumed $\sigma'_{e\ell} \simeq \sigma_{e\ell}$. Also, a factor $\bar{\gamma}$ is introduced in the first term of Eq. (44) to allow for the average geometric probability that a particle receiving enough energy in an elastic collision will actually be ejected from the

atmosphere and not hit the moon and be reflected back into the atmosphere. Following Hinton and Taeusch (Ref. 2) we have taken $\bar{\gamma} = 1$ for the very light gases H, H_2 (which have large scale heights) and $\bar{\gamma} = 1/2$ for the other gases.

The second term of Eq. (44) represents the rate at which an atmospheric particle is lost as the result of a charge exchange collision with an incident solar wind ion. In the collision, the neutral atmospheric particle transfers one or two of its electrons to the incident ion, thereby becoming a positive ion that is swept away by the solar wind and its accompanying magnetic field, before it can recombine in the tenuous atmosphere. However, in analogy with the case of elastic collisions, we must account for those particles that do not actually escape because they are swept toward the lunar surface with sufficient energy to overcome the small positive potential of the surface, are neutralized there and reemitted into the atmosphere. In Hinton and Taeusch's (Ref. 2) notation we let

σ_{ex} = the (measured, calculated or estimated) cross section for the charge exchange scattering of a proton or α particle by an atmospheric gas particle (cf. Table 1),

σ'_{ex} = the charge exchange "escape" cross section,

and the necessary energy to reach the positively charged lunar surface is arbitrarily set equal to the gravitational escape energy. In terms of $\bar{\gamma}$, defined above, $(1 - \bar{\gamma})$ is the average geometric probability that a charge-exchanged particle will hit the lunar surface and $(1 - \bar{\gamma})\sigma'_{ex}$ is the cross section for such particles being reemitted as neutrals to the atmosphere. Thus, the average cross section for actual loss of particles from the atmosphere by the charge exchange mechanism is

$$\sigma_1 = \sigma_{ex} - (1 - \bar{j})\sigma'_{ex} . \tag{45}$$

To calculate σ'_{ex}, it is assumed that

$$\frac{\sigma'_{ex}}{\sigma_{ex}} = \frac{\sigma'_{e\ell}}{\sigma_{e\ell}} , \tag{46}$$

where Table 1 contains the cross sections needed for the calculations. It is seen that, where measurements are available, the difference between H^+ (X = 0.86) and He^{++} (X = 0.14) in charge exchange reactions has been noted.

The third and fourth terms in Eq. (44) represent the photoionization + photodisionization rate and the thermal evaporation rate, respectively, as discussed above in Sec. III.B.1.

The factor β, by which the loss rate terms due to solar wind and photon interactions are multiplied in Eq. (44), is the fraction of the particles of a given species in the atmosphere that is exposed to the sun. The assumed values of β for Model I are listed in Table 1. Since the light particles H and H_2 should have densities that are fairly constant over the lunar surface and also large scale height, h, because of their small mass, most of their scale volume, V, is exposed to the sun. Thus, we take $\beta = 1$ for these. For the heavier particles we have taken $\beta = 1/2$.

To account for the loss due to the interaction between the gas particles and the lunar surface, in this model we may introduce a factor f in Eq. (40) so that the source term D_1 becomes

$$D_1 = \frac{N_A YfM}{W\tau} , \tag{47}$$

where f = the fraction of exhaust gas of a given species that hits the surface and is reemitted in the time τ. Therefore, through the factor f, we can allow for the possibility that a fraction $(1 - f)$ of the impinging exhaust gas sticks to the lunar surface and is not reemitted into the atmosphere. In analogy, similar allowance for sticking to the surface can be made in the first term of B in Eq. (39) and in the second term of A in Eq. (44). However, in the present calculations, in Model I we have assumed no long term sticking of the gas molecules to the lunar surface, i.e., $f = 1$.

3. Model II

Recall that in our present calculations the only atmospheric source considered in this model is the exhaust gas from the descent rockets of the LM (Sec. III.A.3). In addition to the loss rate A, Eq. (44), discussed above, we now wish to allow for losses due to possible adsorption of the exhaust gas on the lunar surface. As discussed above [Eqs. (41c)] we assume that a fraction, f_1, of the impinging, fast moving ($\sim$ 3 km/sec) exhaust gas sticks to the lunar surface upon initial impact and adheres for times long compared to the observation time t.

Furthermore, we assume that in the course of the two dimensional diffusion from the point sources of the thermalized molecules, a fraction, f_2, of these slowly moving molecules adheres to the lunar surface for times long compared to the observation time t. Thus, in this model the loss rate K' [Eqs. (8), (36)] contains in addition to the loss rate A of Eq. (44), a term for the rate of loss due to surface sticking of the diffusing thermalized molecules:

$$K' = - A - \frac{1}{4} \frac{\bar{c} f_2}{h} . \tag{48}$$

The values of the adsorption coefficients f_1 and f_2 for the various gas species in the LM exhaust are listed in Table 2, together with desorption times τ_o. These were calculated (Ref. 11) for chemical adsorption to a silicate model of the lunar surface. The temperature of the lunar surface was taken as constant at 300°K.

Since the true adsorption coefficients and desorption times are dependent upon the nature of the lunar surface material, which is presently unknown, the values of f_1, f_2, and τ_o in Table 2 must be considered as extremely rough estimates only. In our calculations, we have taken $f_1 = f_2 = 0$ for those gas species (H_2, CO, CO_2, H) that have small desorption times ($\lesssim 10^3$ sec), since diffusion theory is not valid for times less than the time it takes a molecule to move through a distance of several mean free paths. For the other gas species in Table 2, which have effectively infinite desorption times, we have performed our calculations with the f_1 and f_2 values listed and also with $f_1 = f_2 = 0$.

In this model we have set $\beta = 1$ in Eq. (44) for all the exhaust species, since for the times and positions of greatest immediate practical interest, (near the LM, within 1 day of landing), the dominant effects probably occur with the bulk of the molecules in sunlight.

Table 2

VALUES OF SOME ADDITIONAL INPUT PARAMETERS FOR MODEL II

Exhaust Species	f_1	f_2	τ_o (sec)	$\bar{c}$ (km/sec)	λ' (10^2 km)†	D' (km^2/sec)
H_2O	0.9750	0.99912	∞	0.645	2.57	39.0
N_2	0.947	0.99885	∞	0.517	1.65	20.1
H_2	0.9926	0.99760	3.2×10^3	1.93	23.0	10.5×10^2
CO	0.874	0.99768	8.7×10^3	0.517	1.65	20.1
CO_2	0.779	0.99767	8.7×10^3	0.412	1.05	10.2
H	0.997	0.99732	1.5×10^2	2.73	46.0	29.6×10^2
OH	0.987	0.99947	∞	0.664	2.72	42.6
NO	0.985	0.99965	∞	0.499	1.54	18.1
O_2	0.933	0.99885	∞	0.483	1.44	16.4
O	0.985	0.99934	∞	0.684	2.89	46.6

†These values were calculated from the equation

$$\lambda' = \frac{\bar{c}^2}{g_m} \sin 2\alpha$$

derived from the laws of kinematics for motion of the thermalized gas particles on a plane surface after they are reemitted with a velocity

$$v = \bar{c} \cos \alpha ,$$

and we have chosen $\alpha = 45°$ as the average angle of reemission.

IV. RESULTS

A. Model I

For each species of the exhaust gas, we have calculated the number density $n(t)$ from Eqs. (3) and (4) for $0 \leq t \leq 10^7$ seconds with $\tau = 100$ and 1000 seconds, $J = 10^9$ and 10^{12} $cm^{-2}sec^{-1}$. In all cases, $T = 300°K$ and $f = 1$. These results are shown in Figs. 5 through 15. In the figures, which are reproductions of CALCOMP plots, the FORTRAN symbols NO(TT) and TT represent $n(t)$ in particles/cm^3 and t in seconds, respectively. Also, f is represented by the FORTRAN symbol F. It should be noted that the number density in each figure is the total of the Hinton and Taeusch (Ref. 2) ambient atmosphere plus the LM exhaust for that particular gas species. Since the log-log plots necessarily distort the values NO(TT) = 0, it should be understood that NO(TT) = 0 at TT = 0 for all the gases except H_2O and H.

B. Model II

For each species of the exhaust gas, we have calculated in Model II $n(\theta,\varphi,t)$ for $10^3 \leq t \leq 10^7$ seconds at several values of θ when $J = 10^9$ cm^{-2} sec^{-1} and $T = 300°K$, for the case of no sticking, $f_1 = f_2 = 0$, and for the case in which the sticking coefficients have the values listed in Table 2. The results are shown in the graphs of Figs. 16-51,† where N(PHE) is the value of $n(\theta,\varphi,t)$ in particles/cm^3, T is the time t in seconds and F_1, F_2 represent f_1, f_2, respectively. Zero time corresponds to the start of the powered descent of LM, which is some 500 seconds before touchdown. It should be noted that the number density,

---

†Figures 16 through 45 are photo reproductions of CALCOMP computer plots made on log-log graph paper using a scale that permits only four cycles on the ordinate axis. This limitation of the mechanical plotter, of course, distorts the curves at large values of T when the N(PHE) values are too small to fit on the scale. Such values are all represented by points plotted on the abscissa axis.

N(PHE), in each figure is that for the LM exhaust only, excluding the Hinton and Taeusch ambient atmosphere. The values 0.001°, 0.01°, 90°, and 180° chosen for θ (indicated by THETA on the figures) correspond to the distances of approximately 30 meters, 300 meters, 2800, and 5600 km, respectively, from the LM touchdown point, which is the pole of our spherical coordinate system.

V. DISCUSSION OF RESULTS

A. Model I

The results presented in Figs. 5-15 for this simple model represent an "averaged" contamination of the lunar atmosphere by the LM exhaust gases. This model should yield the asymptotic values of the contaminant gas densities approached by space dependent distribution models, such as our Model II, at times long after rocket shutoff.

In Model I we have assumed that the total mass of LM exhaust (nominally chosen as 10 metric tons) hits the lunar surface, spreads uniformly over the surface, accommodates to the temperature of the surface (chosen to have a value of 300°K) and is reemitted in its entirety ($f = 1$) into the lunar atmosphere at a constant rate in the time interval τ (chosen as 100 and 1000 seconds). In the actual powered descent phase of the LM, the trajectory of the LM and the exit velocities of the exhaust gases are such that approximately 90 percent of the total exhaust will be lost into space, and of the remaining approximately 10 percent that does strike the surface, some will stick for long periods of time. However, Model II does take cognizance of actual LM descent characteristics and the surface sticking of exhaust particles and, therefore, the results (cf. Figs. 16-51) are more realistic estimates of the intensities and distributions of the LM contaminants in the lunar atmosphere.

In comparing the Model I and Model II results, it should be recalled that our Model I results (Figs. 5-15) give the total of the Hinton and Taeusch ambient atmosphere plus the LM exhaust number density for each gas species in the exhaust, while Model II results (Figs. 16-51) give the number density for the LM exhaust

gas species only. Of the species present in the LM exhaust, H_2O and H are also present in the Hinton Taeusch ambient atmosphere. Furthermore, a total mass of 10 metric tons of exhaust strikes the lunar surface in Model I, while approximately 1 metric ton of exhaust strikes it in Model II. Then, making the appropriate comparisons of the results for Model I (Figs. 5-15) with the results for Model II (Figs. 16-46), at times after a uniform distribution has been reached, it is seen that Model II number densities do approach the Model I densities. [H_2 is an exception, which is probably due to the crude $\beta(= 1)$ value chosen for it in Model II]. For example, in Fig. 46 the densities (in cm^{-3}) of CO are plotted against the time (in secs) for Models I and II. We have scaled the Model I densities down by a factor of 1/10 to account for the 10 times larger initial total mass of exhaust assumed in Model I. It is clear that Model II densities approach those of Model I after some few days, when a uniform distribution over the surface is attained in Model II.

It is seen from Figs. 5-15 that H_2O, N_2, and CO make the largest contributions in this simple model over periods greater than 1 day. If a total mass of 10 metric tons of exhaust strikes the lunar surface, water vapor, the contaminant of greatest selenophysical interest, reaches a maximum particle density of approximately 20 times that predicted (Ref. 2) for its abundance in the ambient atmosphere. It is clear from the figures that, except for hydrogen (H), the effect of an increase in the solar wind flux (J) is to decrease the density and decay times of the contaminants. The solar wind tends to sweep the atmosphere clean of all contaminants except H. In the case of H, the solar wind protons (H^+) are neutralized and diffusely reflected by the lunar surface and thus add to the H content of the atmosphere. This effect, of course, increases with an increase in solar wind flux. For con-

venience of comparison, we have plotted in Fig. 5 the Model I densities (in cm^{-3}) of H_2O, H, and O_2 against the time (in secs) for $J = 10^9$ and $J = 10^{12}$ ($cm^{-2}sec^{-1}$) for $\tau = 1000$ secs.

Figure 6 compares the Model I densities of atomic oxygen for two values of τ ($= 10^2$, 10^3 secs) and $J(= 10^9, 10^{12}$ particles/cm^2 sec). Figure 7 makes the same comparisons for water vapor. The behavior with τ exhibited in Fig. 6 and discussed in Sec. II.A.3 above is characteristic of the densities of all the exhaust species for which $B = 0$ ($= n_o$), i.e. all species except H_2O and H. For brevity we have not included in this report the figures for the remaining species in Table 1 when $\tau = 100$ secs.

B. Model II

For this more realistic model, the space and time distributions of the particle number densities for the LM contaminant gases in the lunar atmosphere are shown in Figs. 16-51. Results are obtained for the region of prime interest for the first Apollo mission, that is, within 300 meters of LM touchdown, for a simulated LM descent trajectory that lies wholly in the plane of a lunar great circle. This was chosen as the lunar meridional plane, i.e., the $\varphi = 0$ plane. Results are also shown for the particle densities at large distances (up to 5600 km) from the LM touchdown point. The total mass of the LM exhaust gases was arbitrarily chosen as 10 metric tons, of which 1 metric ton reaches the surface of the moon from the far-field gas flow. This is confined almost exclusively to the region enclosed by the 10° latitude circle about the LM touchdown point (pole).† The number density calculations were performed 1) using

†See Table 11, p. 60 of Ref. 11.

the sticking coefficients in Table 2 and, also 2) under the assumptions of no sticking to the lunar surface. The sticking coefficients used (Table 2) were obtained from Sec. IV.F and G of Ref. 11. We have included only chemical sticking since the physical sticking coefficients have desorption times that are very short (~ several seconds) compared to the relatively long times ($\lambda'/\bar{c} \sim 10^3$ seconds) needed for the diffusion equation [Eq. (8)] to be applicable.

It is clear from Fig. 50 and Figs. 16-44 that the single most important loss mechanism is that of adsorption to the lunar surface. Unfortunately, this effect is probably also the least well known of the loss mechanisms, due to the general lack of knowledge of the physical and chemical properties of the lunar surface. This, combined with the fact that the solar wind itself is not well known, makes the theoretical determination of the structure of the lunar atmosphere and its contamination very uncertain, and at best only order of magnitude estimates can be expected.

In Model II, only the far-field input has been considered since estimates of the near-field contribution to the atmosphere indicate that it is small compared to the far-field contribution.

The results presented in Figs. 16-51 are for a solar wind flux of 10^9 positive ions per cm^2 per second, which approximates average solar wind parameters. However, since the first Apollo mission will be near the time of solar maximum, it is anticipated that the solar wind will be more intense than average. Larger solar wind fluxes will lead to smaller decay times for the exhaust contaminants and thereby effect a faster removal of the contaminants from the lunar atmosphere.

For both models, the values of the parameter $\bar{\gamma}$ chosen for each gas species are given in Table 1. We recall that this parameter is an attempt to represent the geometric probability that a

particle receiving enough energy in a collision to enable it to escape will actually escape and therefore be lost to the atmosphere. Following the reasoning of Hinton and Taeusch in Ref. 2, we have chosen $\bar{\gamma} = 1$ for the light gases H and H_2, and $\bar{\gamma} = 1/2$ for the remaining heavy gases in the LM exhaust.

In Model II we have chosen $\beta = 1$ for all the exhaust gas species. This parameter represents the fraction of the particles in the atmosphere that are exposed to the sun. As distinguished from Model I, where the exhaust gases were assumed uniformly distributed over the lunar surface so that $\beta = 1/2$ was chosen as a reasonable value (except for the light gases H and H_2 where $\beta = 1$ was chosen), the values of $\beta = 1$ in Model II account for the fact that the gases, except H and H_2, diffuse slowly from the sunlit side (where LM in the first Apollo mission will land) to the dark side. For H and H_2, which diffuse quickly, the value $\beta = 1$ is probably crude. In fact, in the case of H, which has in addition to the LM exhaust source an additional source due to neutralization of the solar wind protons, there should probably be two parameters β instead of one.

The values of the cross sections listed in Table 1 are reasonable estimates gleaned from the limited literature on these collision processes. The literature is particularly scant on photodissociation cross sections, so that these were estimated from the more abundant literature on total photoabsorption cross sections.

Finally, it should be pointed out that the results for very early times ($\lesssim 10^3$ sec) are not valid, since for the diffusion theory to apply the gas molecule must have undergone at least several hops along the surface.

The present calculations have shown that:

a) For a given latitude (θ) on the lunar surface, the particle density for any atmospheric contaminant species is not a function of the longitude φ. For example, see Fig. 47 where the density of H_2O is plotted for $\theta = 90°$ and $\varphi = 0°, 90°, 180°$. The other exhaust species exhibit a similar φ behavior. Thus the Model II results presented in all the other figures are at $\varphi = 0°$.

b) In the region of LM touchdown, the particle density of the contaminants in the atmosphere does not change with distance for distances of 30 meters to 300 meters from touchdown. Therefore, the graphs for 30 meters ($\theta = 0.001°$) are identical to those for 300 meters ($\theta = 0.01°$), which are shown in the figures below.

It is seen from Fig. 48 and from Figs. 16-45, by comparing the densities for the no sticking ($f_1 = f_2 = 0$) cases near the ($\theta = 0.01°$) with those at large distances ($\theta = 90°, 180°$), that the light molecules H (Figs. 31-33) and H_2 (Figs. 22-24) are uniformly distributed in the atmosphere over the moon's surface in a couple of hours, while the heavier contaminants, CO_2 (Figs. 28-30) and O_2 (Figs. 40-42), require approximately six days to attain such a uniform distribution. The other contaminants have distribution times between these extremes with that of H_2O being approximately two days. It is also clear that for the case of no sticking, the particle number densities of the contaminants are sufficiently large for significantly long times both in the vicinity of LM touchdown (Fig. 49) and also at great distances that they should be readily detectable by standard instruments. Indeed, if the present

experimental and theoretical estimates (Refs. 2, 12) of approximately 10^6 particles/cm^3 for the ambient lunar atmosphere are correct, and there is no sticking of the exhaust contaminants to the surface, then the total particle number density of the contaminants in the vicinity of the LM is of the order of the ambient atmosphere for the first day after touchdown (Fig. 51).† However, in the event that sticking to the surface occurs to the extent that we have estimated, those contaminants which have nonzero sticking coefficients (H, O, N_2, OH, NO, O_2, O) will be detectable in the atmosphere only by more sensitive instruments in the vicinity of LM touchdown and then only during the first few hours after touchdown (Fig. 50). After this time period, only trace amounts ($< 10^{-4}$ particles/cm^3) of such contaminants will be present in the lunar atmosphere. At great distances from the LM touchdown, such contaminants will never be present in more than trace amounts. The contaminants H, H_2, CO, and CO_2 with zero sticking coefficients will predominate in the lunar atmosphere, with CO and CO_2 being most prevalent and most persistent.

---

† In this figure, the curves are obtained by summing the calculated densities of all the LM exhaust species for the cases of

(a) no sticking: $f_1 = f_2 = 0$ for all species,

(b) sticking: f_1, f_2 have the values listed in Table 2,

and plotting these against time. The major contributions to the "sticking" curve are from those species (H_2, CO, CO_2, H) that have zero sticking coefficients (Table 2). The "Total Ambient" and "Ambient $H + H_2O$" lines are obtained from the steady state calculations of Hinton and Taeusch (Ref. 2).

Finally, the amount of atmospheric contamination for other values of the sticking coefficients can be estimated roughly from the figures (except for H, H_2, CO, CO_2). In addition to the cases of zero sticking and large sticking, there is the additional (trivial) case of complete sticking, $f_1 = f_2 = 1.0$, which corresponds to zero atmospheric contamination (except for a small orbital component that decays with the time constant A^{-1}) at all times after the first contact of the LM exhaust gases with the surface. Thus, it is possible to interpolate roughly between these three values of the sticking coefficients to find the contamination for intermediate sticking values.

C. Approximate Formula

It is possible to obtain a simple approximate form for the atmospheric density [Eq. (38)] of the various contaminant species in the LM exhaust. We start by assuming that the LM exhaust that strikes the lunar surface is concentrated at the LM touchdown site ($\theta = 0°$, $\varphi = 0°$), so that it constitutes a single point source for the atmosphere. Since there is now only one point source at

$$\begin{aligned} &\theta_i = 0°, \ \varphi_j = 0°, \\ &q_{oijk} = q_o, \\ &\cos\alpha = \cos\theta = \mu, \end{aligned} \tag{49}$$

and using Eq. (36), Eq. (37) takes the explicit form

$$n'(\theta,\varphi,t) = \frac{q_o}{2} e^{-|K'|(t-t_k)} U'(t-t_k) \sum_{\ell=0}^{\infty} (2\ell+1) P_\ell(\mu) \, e^{-a\ell(\ell+1)} , \tag{50}$$

where

$$a = \frac{D'}{r_o^2}(t - t_k) \ . \tag{51}$$

When a is small ($\lesssim 1$), taking ℓ as a continuous rather than a discrete parameter, Eq. (50) can be approximated by

$$n'(\theta,\varphi,t) \approx \frac{q_o}{2} e^{-|K'|(t-t_k)} U'(t - t_k) \int_0^\infty (2\ell + 1) P_\ell(\mu) \ e^{-a\ell(\ell+1)} \ d\ell \ .$$

For an observer in the vicinity of the LM touchdown site, $\theta \approx 0°$, $\varphi \approx 0°$,

$$n'(0°,0°,t) \approx \frac{q_o}{2} e^{-|K'|(t-t_k)} U'(t - t_k) \int_0^\infty (2\ell + 1) \ e^{-a\ell(\ell+1)} \ d\ell \ ,$$

$$\approx \frac{q_o}{2} e^{-|K'|(t-t_k)} U'(t - t_k) \left(-\frac{1}{a}\right) \int_0^\infty \frac{d}{d\ell} e^{-a\ell(\ell+1)} \ d\ell \ ,$$

$$n'(0°,0°,t) \approx \frac{q_o}{2a} e^{-|K'|(t-t_k)} U'(t - t_k) \ . \tag{52}$$

Substituting Eq. (52) for the surface density (in cm^{-2}) into Eq. (38), we obtain the approximate formula for the volume density (in cm^{-3}) in the vicinity of the LM touchdown site:

$$n(r,0°,0°;\ t) \approx \frac{q_o r_o^2}{2hD'} \frac{e^{-|K'|(t-t_k)}}{(t - t_k)} U'(t - t_k) , \tag{53}$$

where h is the scale height (in cms) of a given species of LM exhaust gas and q_o is the strength (in molecules/cm^2) of the single source for this species placed at the LM touchdown point.

To determine q_o, consider a total mass, M (in gms), of exhaust gas striking the surface so that the number of molecules of a given specie reemitted is given by

$$\frac{MN_A Y}{W} (1 - f_1) . \tag{54a}$$

Representing the single point source for a given specie by

$$q(\mu,\varphi,t) = q_o \delta(\mu)\delta(\varphi - \varphi_j)\delta(t - t_k) , \tag{54b}$$

an expression for q_o is obtained by equating the total number of molecules emitted as expressed by (54a) and by the integral of Eq. (54b) over the time variable and over the surface of the moon:

$$\frac{MN_A Y}{W} (1 - f_1) = \iiint q_o \delta(\mu)\delta(\varphi - \varphi_j)\delta(t - t_k) r_o^2 \, d\mu d\varphi dt$$

yielding q_o in molecules per cm^2:

$$q_o \approx \frac{MN_A Y}{r_o^2 W} (1 - f_1) . \tag{55}$$

Since $a \lesssim 1$, from Eq. (51) and Table 2 it is clear that the approximate formula, Eq. (53), holds for $10^3 \lesssim t - t_k \lesssim 10^5$ for all the exhaust gas species except H and H_2, in which case $10^3 \lesssim t - t_k \lesssim 10^4$, where the lower limit in both cases, $t - t_k \gtrsim 10^3$ secs, follows from the fact that the diffusion theory is applicable only for times greater than the mean time ($\lambda'/\bar{c} \sim 10^3$ seconds) between impacts of the diffusing particles with the lunar surface.

It was found that Eq. (53) gives better than order of magnitude agreement with the computer calculations of the atmospheric density of the LM exhaust species in the vicinity of the LM touchdown point.

VI. REFERENCES

1. Morse, P. M. and Feshbach, H., Methods of Theoretical Physics, Chap. 10, McGraw-Hill, 1953.

2. (a) Hinton, F. L. and Taeusch, D. R., The Lunar Atmosphere, Scientific Report KS-1, University of Michigan Research Institute, October 1962.

   (b) _____ "Variation of the Lunar Atmosphere with the Strength of the Solar Wind," J. Geophys. Res., Vol. 69, p. 1341, 1964.

3. Singer, S. F., "Atmosphere Near the Moon," Astronaut. Acta, Vol. 7, p. 135, 1961.

4. Opik, E. J. and Singer, S. F., "Escape of Gases from the Moon," J. Geophys. Res., Vol. 65, p. 3065, 1960.

5. Herring, J. R. and Licht, A. L., "Effect of the Solar Wind on the Lunar Atmosphere," Science, Vol. 130, p. 266, 1959.

6. Gold, T., in discussion following R. Jastrow, "Outer Atmospheres of the Earth and Planets," J. Geophys. Res., Vol. 64, p. 1798, 1959.

7. Edwards, W. F. and Borst, L. B., "Possible Sources of a Lunar Atmosphere," Science, Vol. 127, p. 325, 1958.

8. Vestine, E. H., Evolution and Nature of the Lunar Atmosphere, Rand Corp. Res. Mem. RM-2106, January 1958.

9. Watson, K., Murray, B. C., and Brown, H., "The Behavior of Volatiles on the Lunar Surface," J. Geophys. Res., Vol. 66, p. 3033, 1961.

10. Aller, L. H., The Abundance of the Elements, Interscience Publishers, New York, p. 192, 1961.

11. Aronowitz, L., et al., Investigation of Lunar Surface Chemical Contamination by LEM Descent Engine and Associated Equipment, Grumman Research Department Report RE-242, March 1966, final report on Contract NAS 9-4860.

12. Elsmore, B., "Radio Observations of the Lunar Atmosphere," Phil. Mag., Vol. 2, p. 1040, 1957.

13. Hinterreger, H. E., "Interplanetary Ionization by Solar Extreme Ultraviolet Radiation," Ap. J. Vol. 132, p. 801, 1960.

14. Jeans, J. H., The Dynamical Theory of Gases, 4th ed., Dover Publications, New York, 1954.

15. Allison, S. K. and Garcia-Munoz, M., "Electron Capture and Loss at High Energies," Chap. 19 in Atomic and Molecular Processes, edited by D. R. Bates, Academic Press, New York and London, 1962.

16. Wainfan, N., Walker, W. C., and Weissler, G. L., "Photoionization Efficiencies and Cross Sections in O_2, N_2, CO_2 A, H_2O, H_2, and CH_4," Phys. Rev., Vol. 99, p. 542, 1955.

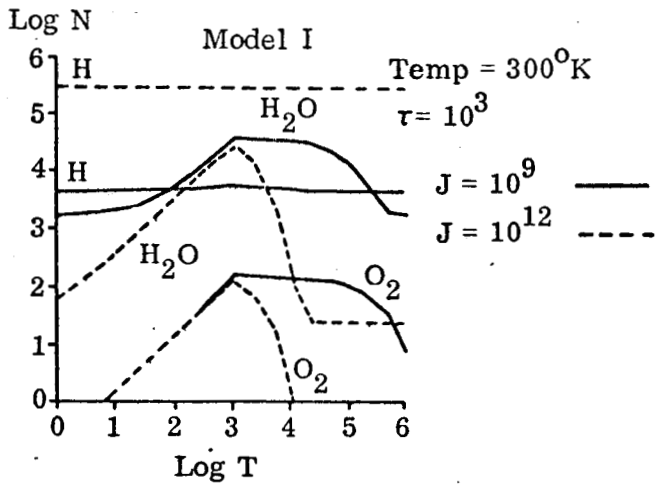

Fig. 5 H_2O, H, O_2 — Comparison of Model I Results (Number of Particles/cm^3 versus Time in Seconds) for $J = 10^9$ with $J = 10^{12}$

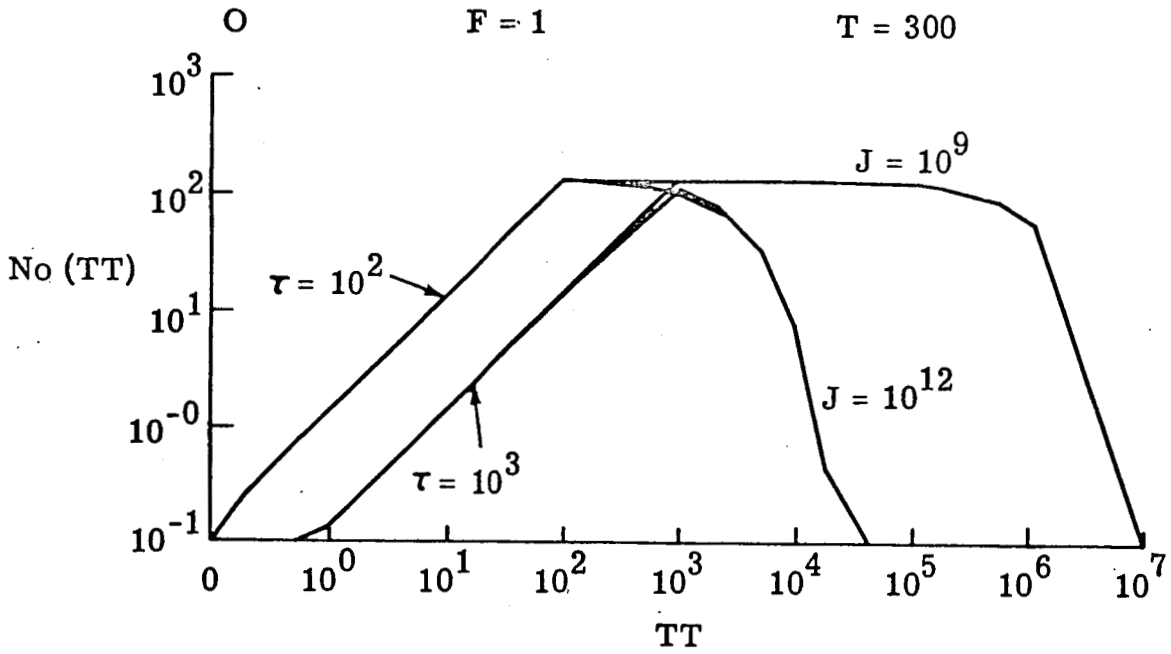

Fig. 6 O — Comparison of Model I Results (Number of Particles/cm^3 versus Time in Seconds) for Two Different Values of the Parameters τ and J

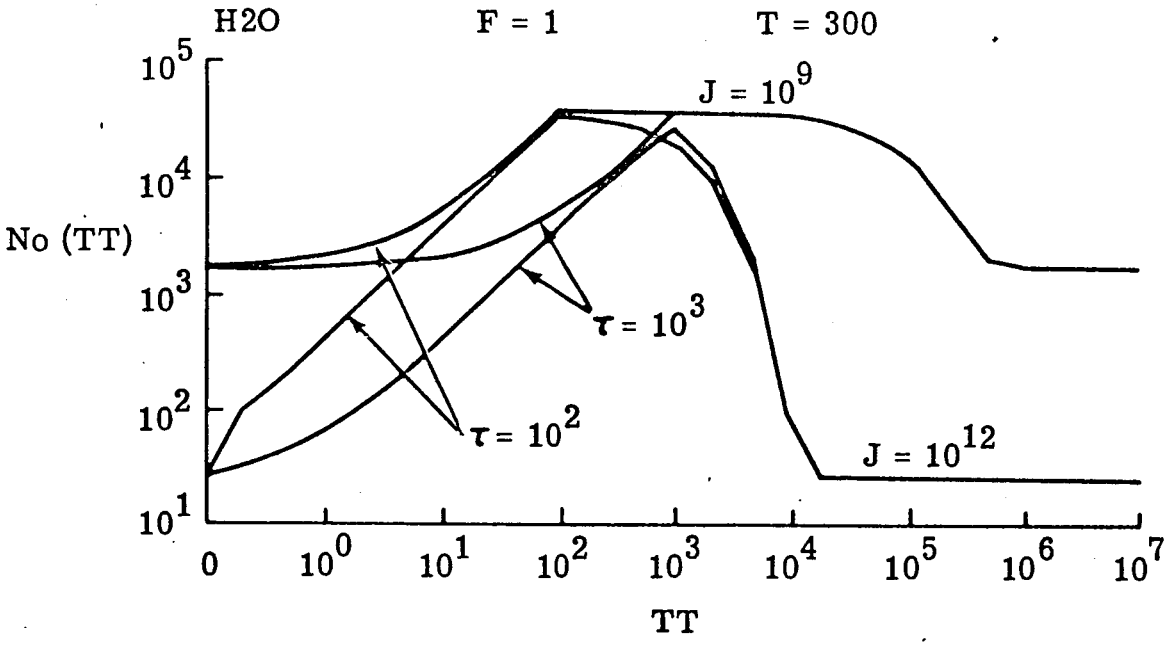

Fig. 7 H_2O — Comparison of Model I Results (Number of Particles/cm^3 versus Time in Seconds) for Two Different Values of the Parameters τ and J

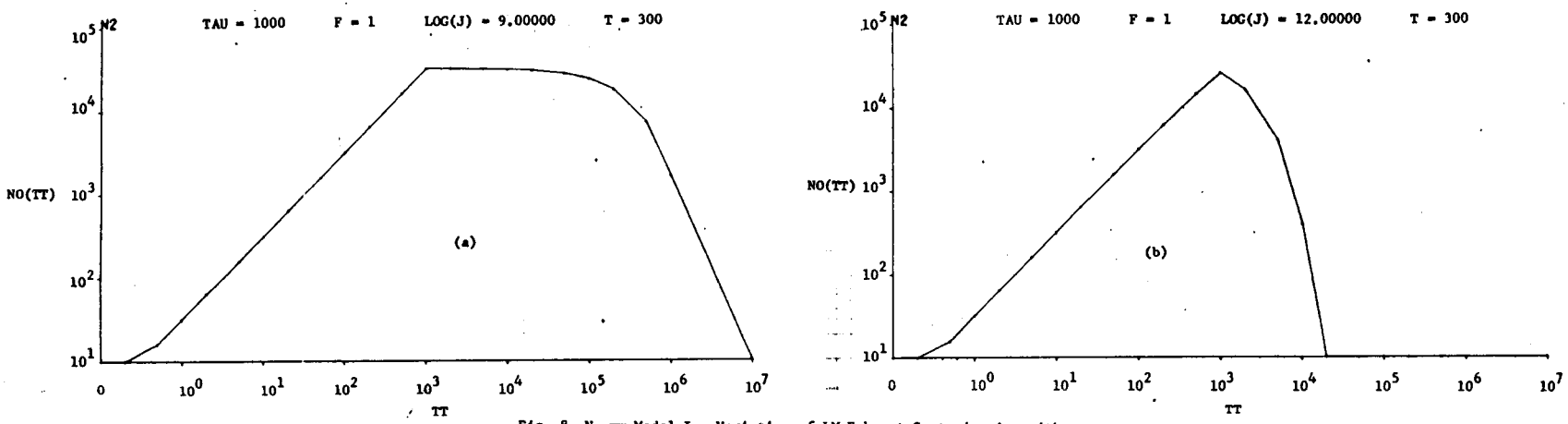

Fig. 8 N_2 — Model I. Variation of LM Exhaust Contamination with Time (Number of Particles/cm^3 versus Time in Seconds) for (a) $J = 10^9$, (b) $J = 10^{12}$

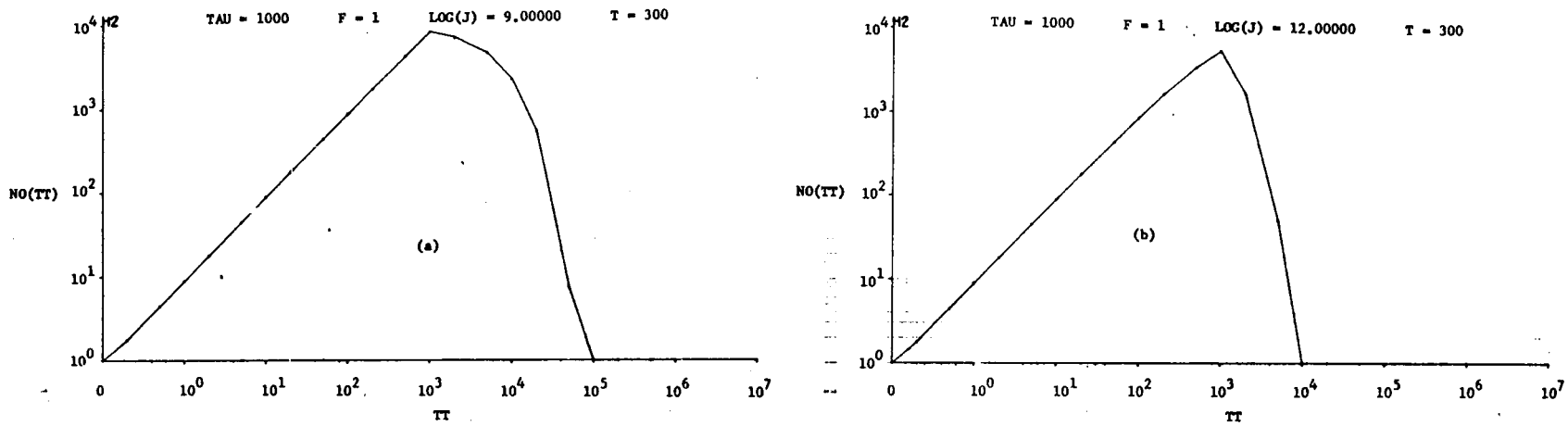

Fig. 9 H_2 — Model I. Variation of LM Exhaust Contamination with Time (Number of Particles/cm^3 versus Time in Seconds) for (a) $J = 10^9$, (b) $J = 10^{12}$

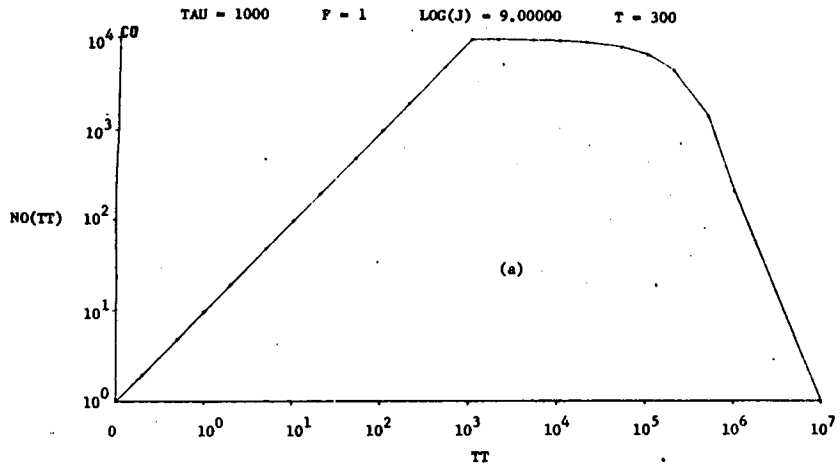

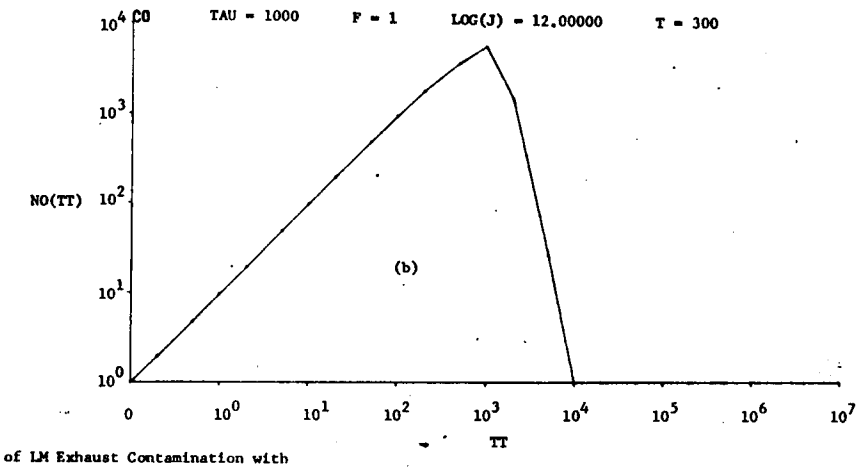

Fig. 10 CO — Model I. Variation of LM Exhaust Contamination with Time (Number of Particles/cm^3 versus Time in Seconds) for (a) $J = 10^9$, (b) $J = 10^{12}$

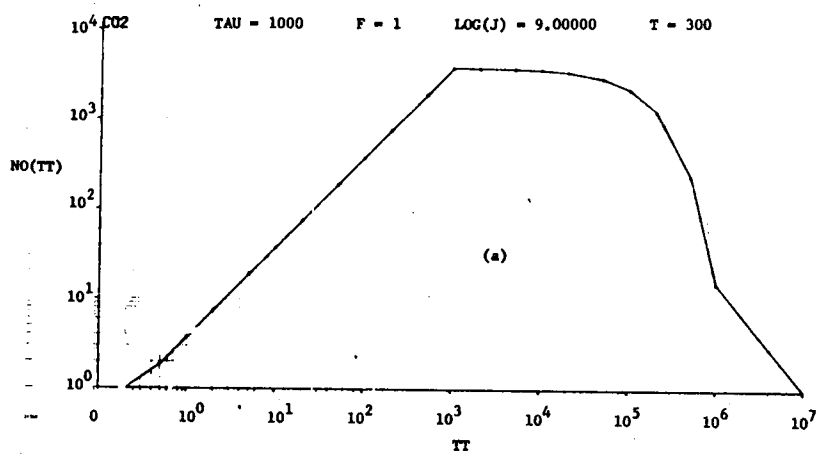

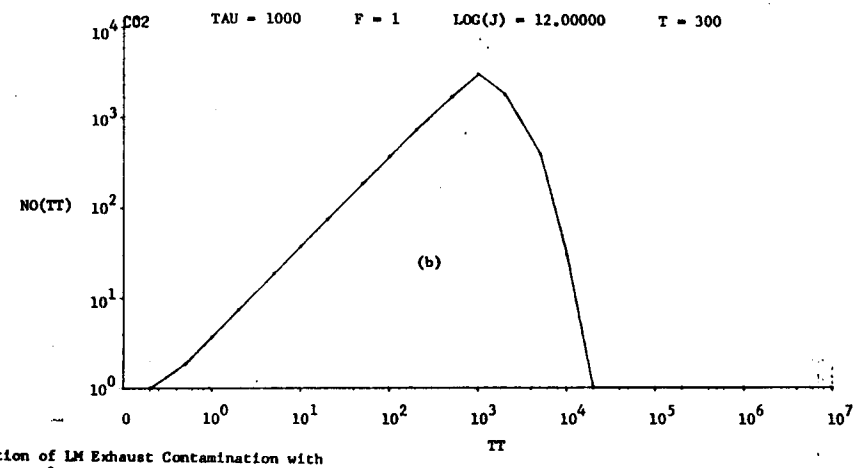

Fig. 11 CO_2 — Model I. Variation of LM Exhaust Contamination with Time (Number of Particles/cm^3 versus Time in Seconds) for (a) $J = 10^9$, (b) $J = 10^{12}$

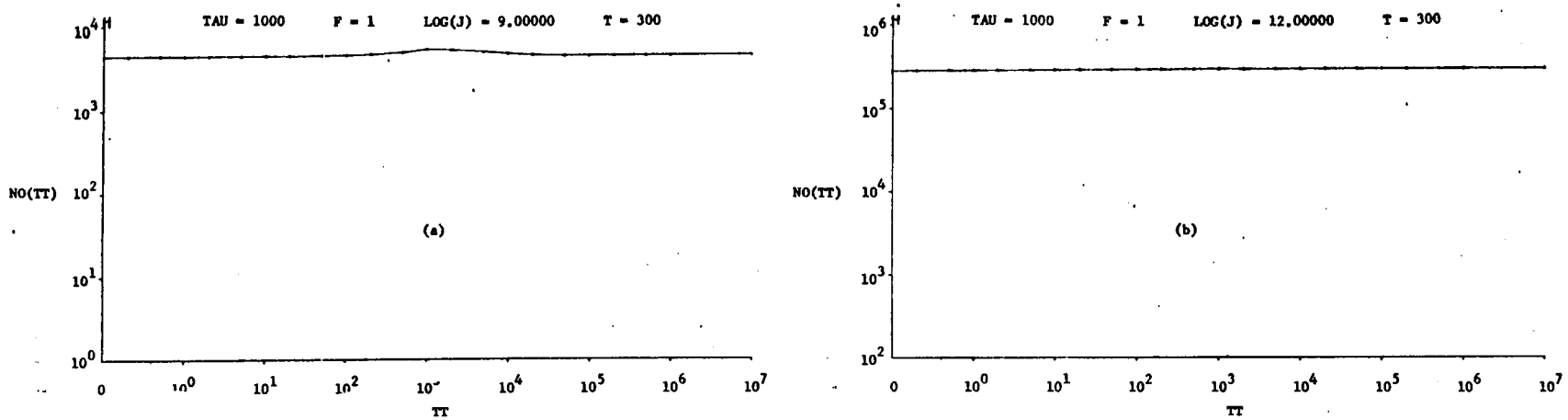

Fig. 12 H — Model I. Variation of LM Exhaust Contamination with Time (Number of Particles/cm^3 versus Time in Seconds) for (a) $J = 10^9$, (b) $J = 10^{12}$

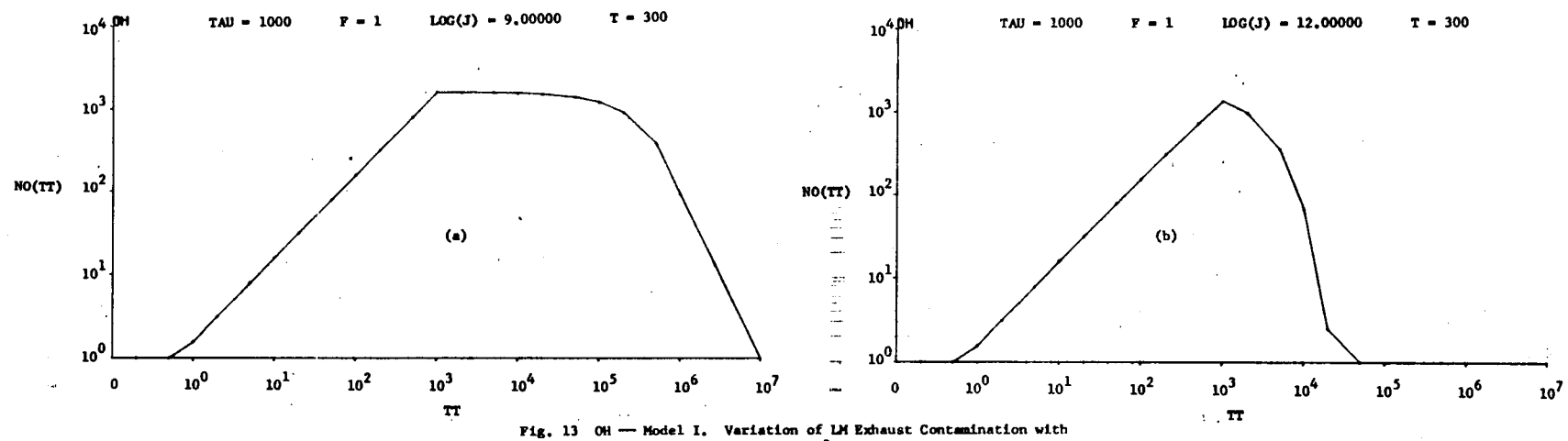

Fig. 13 OH — Model I. Variation of LM Exhaust Contamination with Time (Number of Particles/cm^3 versus Time in Seconds) for (a) $J = 10^9$, (b) $J = 10^{12}$

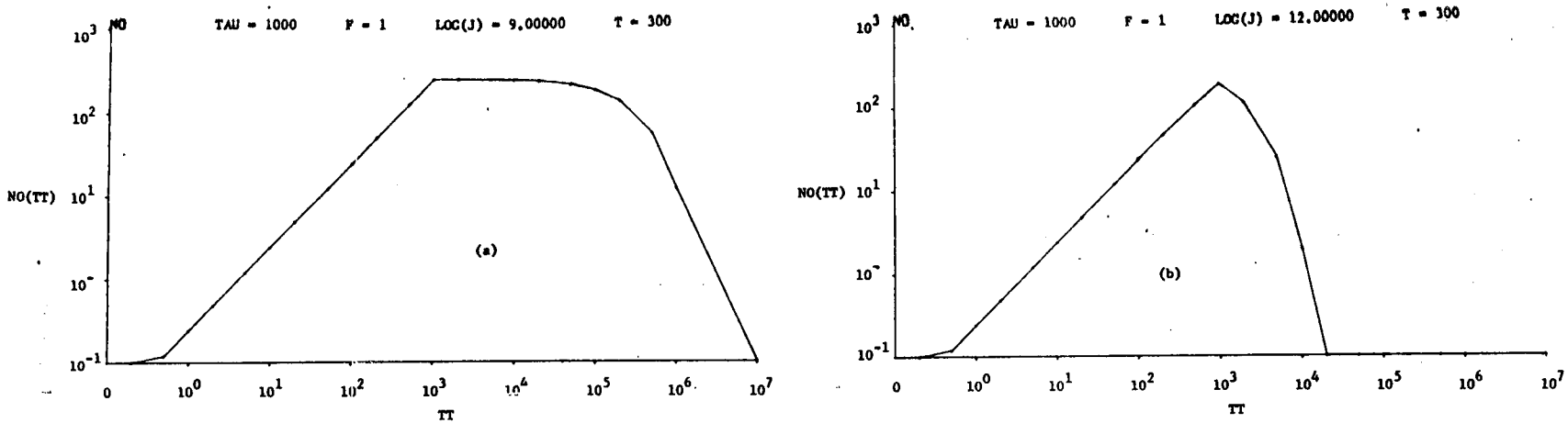

Fig. 14 NO — Model I. Variation of LM Exhaust Contamination with Time (Number of Particles/cm^3 versus Time in Seconds) for (a) $J = 10^9$, (b) $J = 10^{12}$

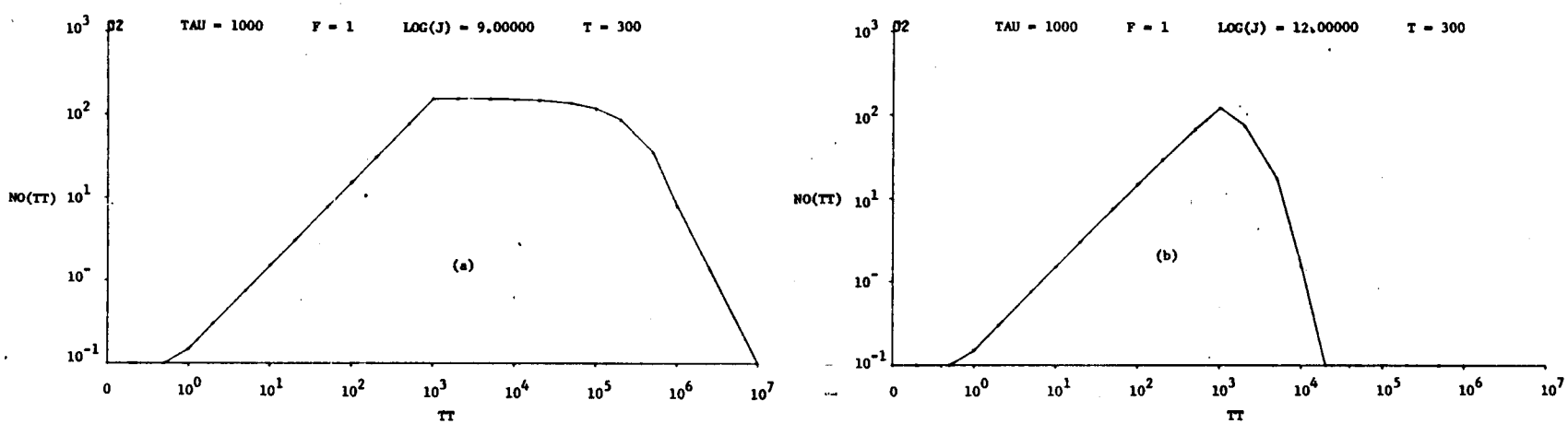

Fig. 15 O_2 — Model I. Variation of LM Exhaust Contamination with Time (Number of Particles/cm^3 versus Time in Seconds) for (a) $J = 10^9$, (b) $J = 10^{12}$

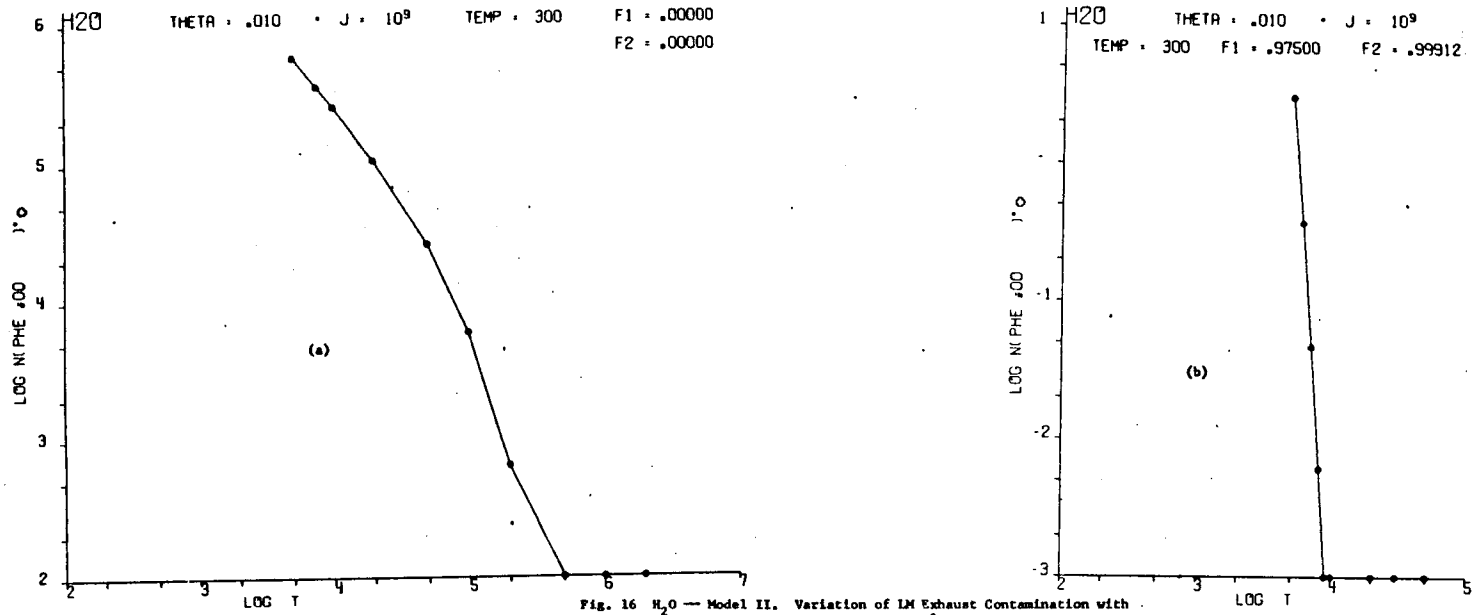

Fig. 16 H_2O — Model II. Variation of LM Exhaust Contamination with Time (Log of Number of Particles/cm^3 versus Log of Time in Seconds) at 30 to 300 Meters from LM Touchdown for (a) No sticking, (b) Sticking

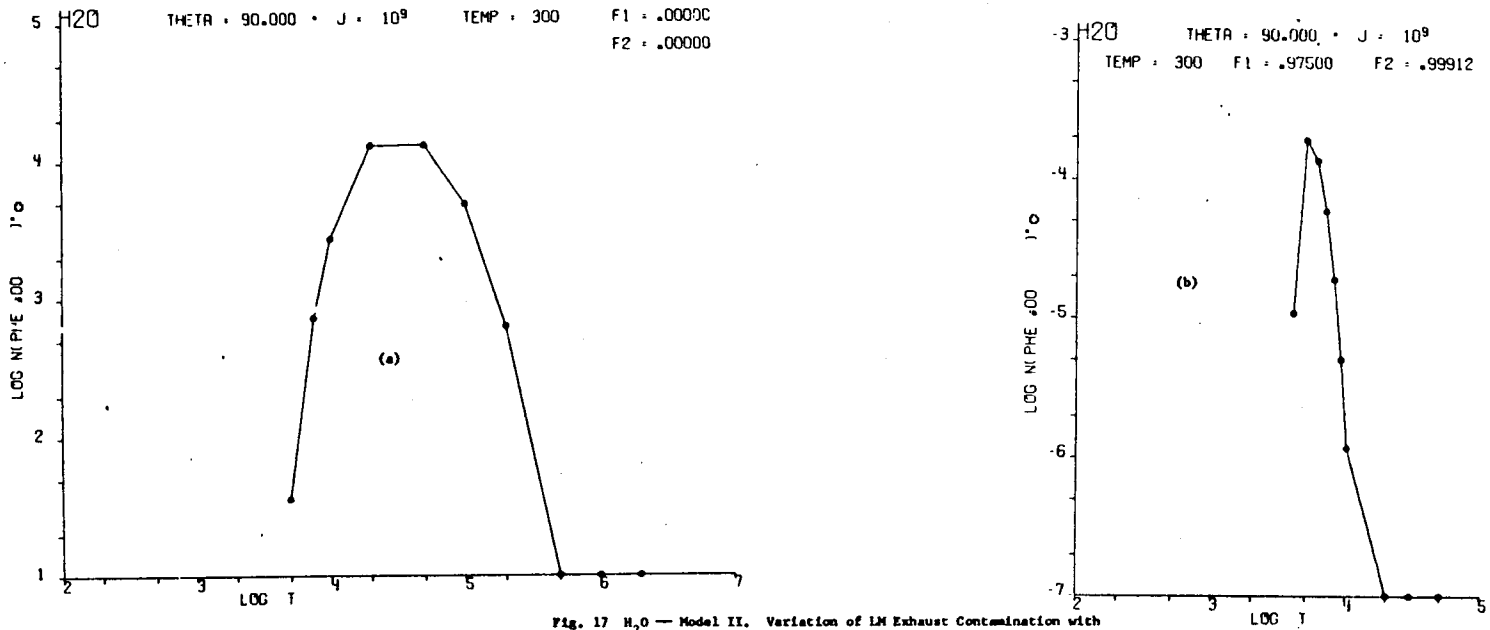

Fig. 17 H_2O — Model II. Variation of LM Exhaust Contamination with Time (Log of Number of Particles/cm^3 versus Log of Time in Seconds) at 2700 km from LM Touchdown for (a) No Sticking, (b) Sticking

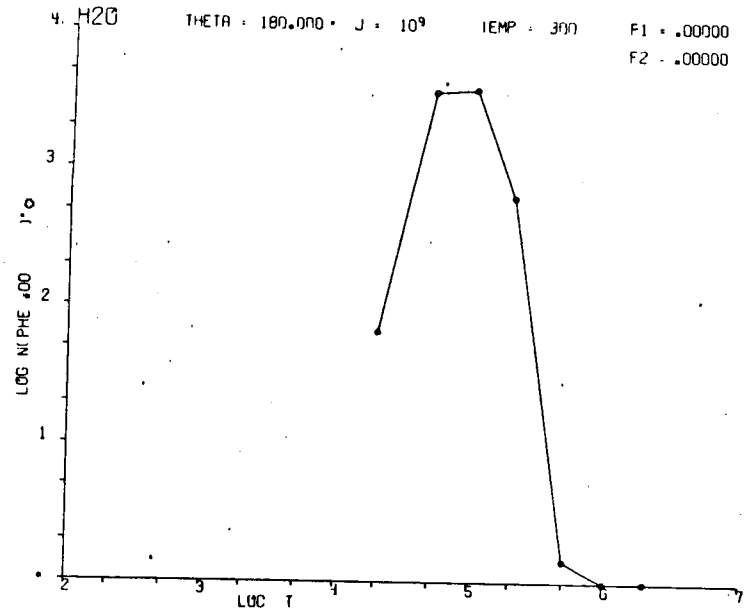

Fig. 18 H_2O — Model II. Variation of LM Exhaust Contamination with Time (Log of Number of Particles/cm^3 versus Log of Time in Seconds) at 5600 km from LM Touchdown for No Sticking

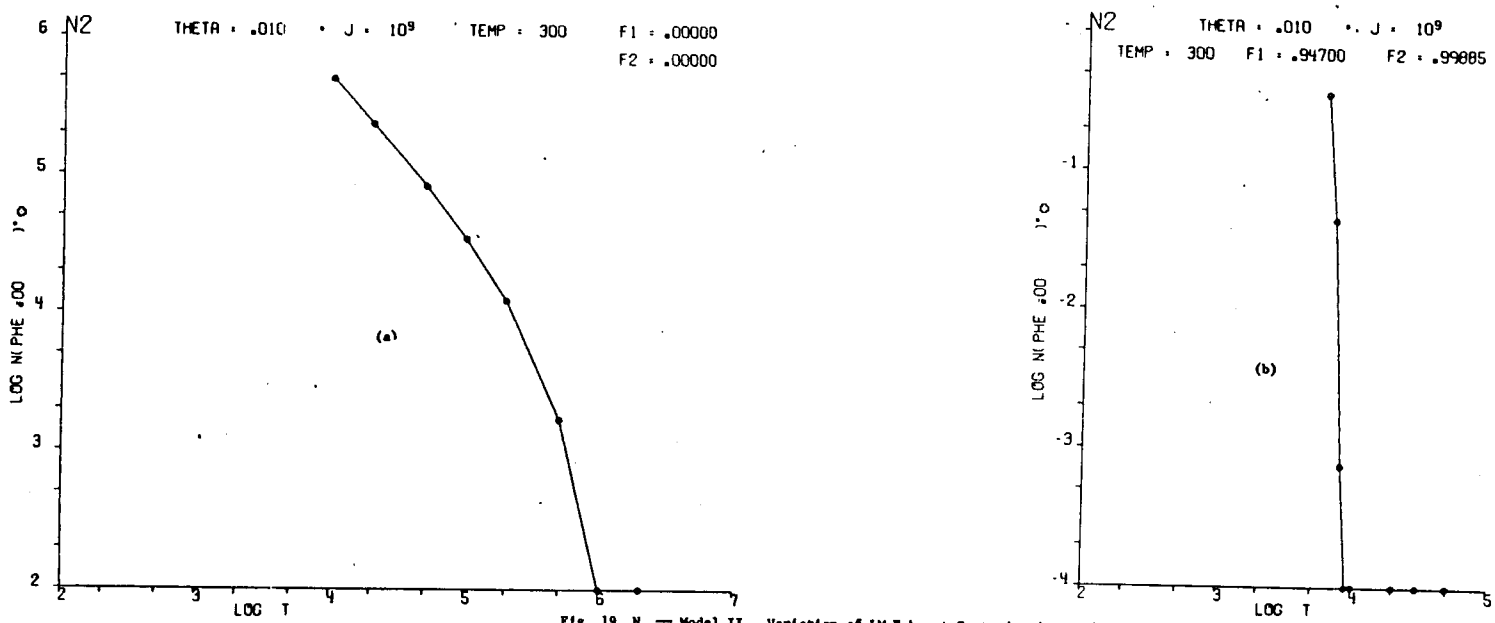

Fig. 19 N_2 — Model II. Variation of LM Exhaust Contamination with Time (Log of Number of Particles/cm^3 versus Log of Time in Seconds) at 30 to 300 Meters from LM Touchdown for (a) No Sticking, (b) Sticking

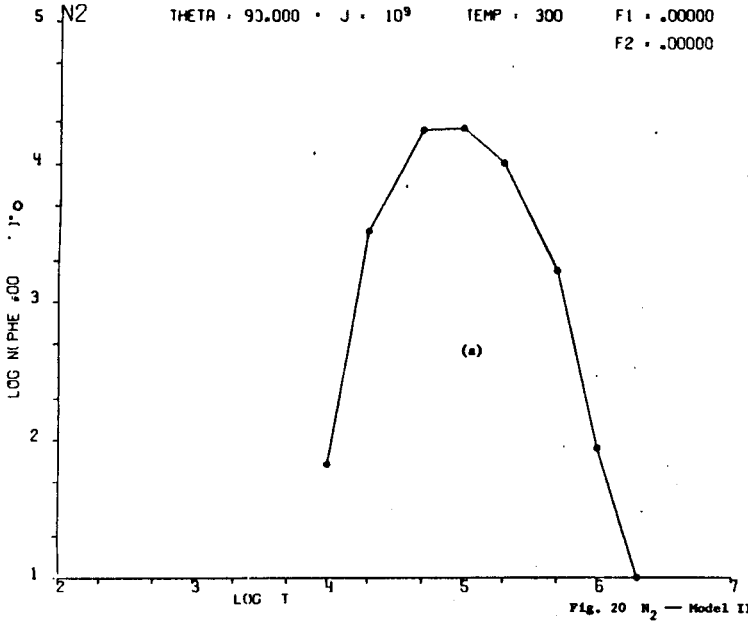

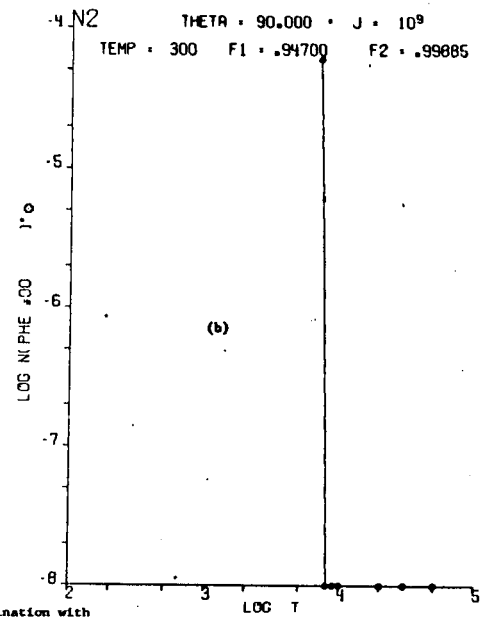

Fig. 20 N_2 — Model II. Variation of LM Exhaust Contamination with Time (Log of Number of Particles/cm^3 versus Log of Time in Seconds) at 2700 km from LM Touchdown for (a) No Sticking, (b) Sticking

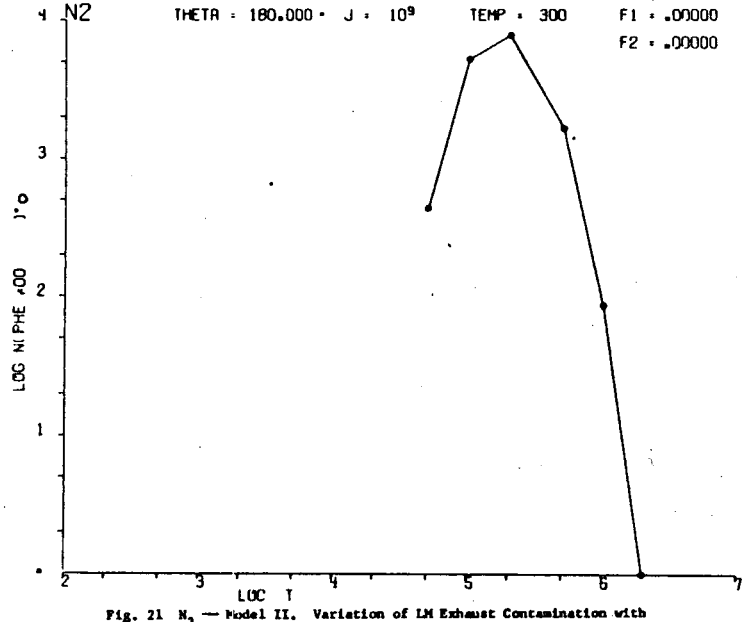

Fig. 21 N_2 — Model II. Variation of LM Exhaust Contamination with Time (Log of Number of Particles/cm^3 versus Log of Time in Seconds) at 5600 km from LM Touchdown for No Sticking

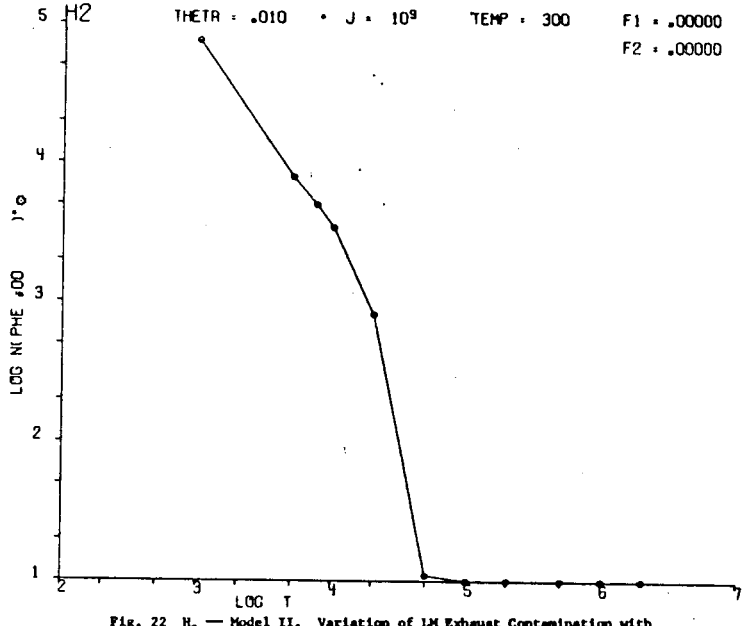

Fig. 22 H_2 — Model II. Variation of LM Exhaust Contamination with Time (Log of Number of Particles/cm^3 versus Log of Time in Seconds) at 30 to 300 Meters from LM Touchdown for No Sticking

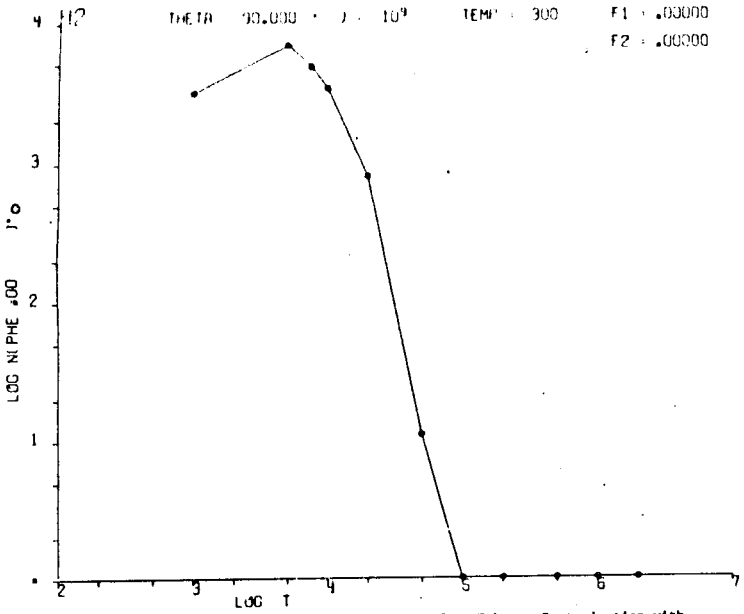

Fig. 23 H_2 — Model II. Variation of LM Exhaust Contamination with Time (Log of Number of Particles/cm^3 versus Log of Time in Seconds) at 2700 km from LM Touchdown for No Sticking

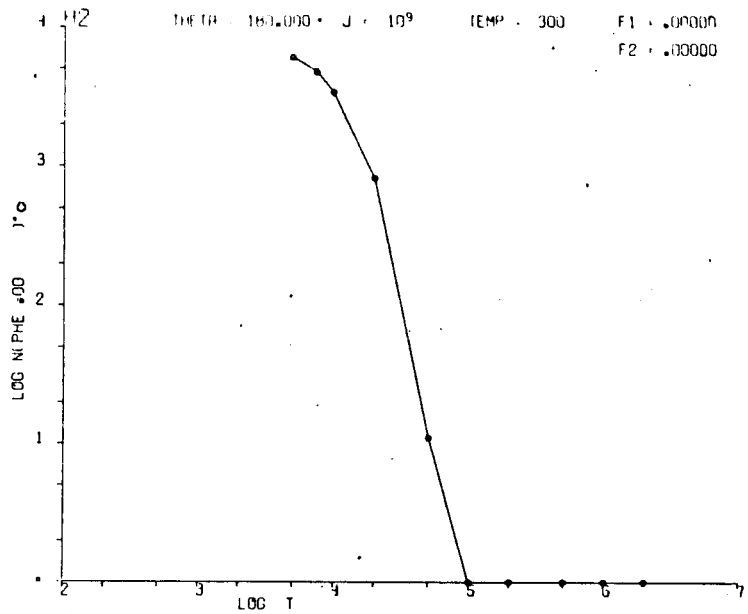

Fig. 24 H_2 — Model II. Variation of LM Exhaust Contamination with Time (Log of Number of Particles/cm^3 versus Log of Time in Seconds) at 5600 km from LM Touchdown for No Sticking

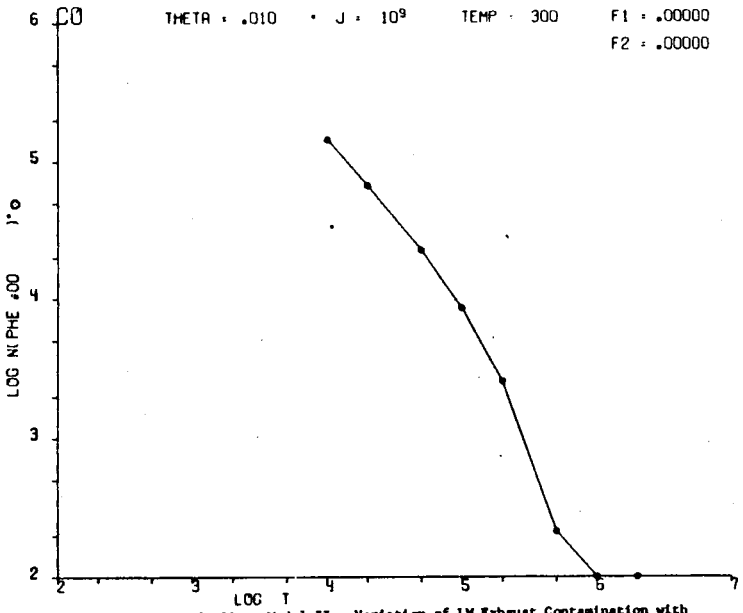

Fig. 25 CO — Model II. Variation of LM Exhaust Contamination with Time (Log of Number of Particles/cm^3 versus Log of Time in Seconds) at 30 to 300 Meters from LM Touchdown for No Sticking

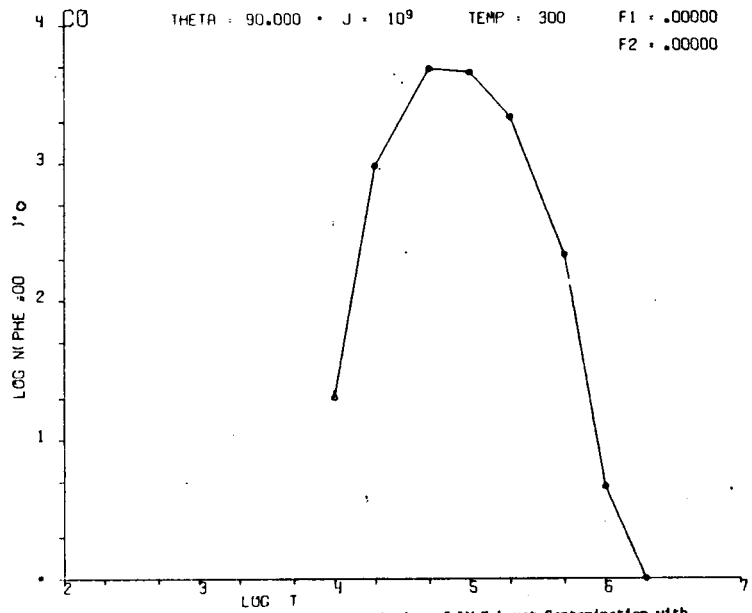

Fig. 26 CO — Model II. Variation of LM Exhaust Contamination with Time (Log of Number of Particles/cm^3 versus Log of Time in Seconds) at 2700 km from LM Touchdown for No Sticking

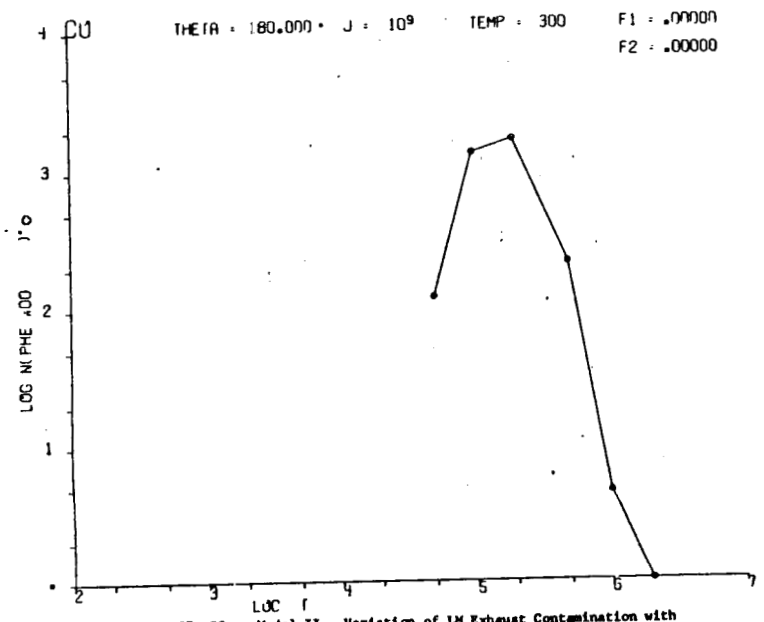

Fig. 27 CO — Model II. Variation of LM Exhaust Contamination with Time (Log of Number of Particles/cm^3 versus Log of Time in Seconds) at 5600 km from LM Touchdown for No Sticking

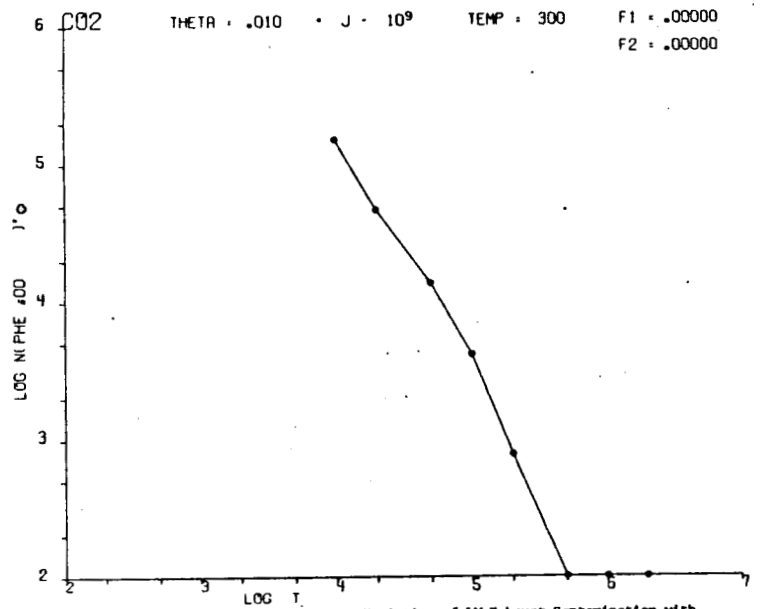

Fig. 28 CO_2 — Model II. Variation of LM Exhaust Contamination with Time (Log of Number of Particles/cm^3 versus Log of Time in Seconds) at 30 to 300 Meters from LM Touchdown for No Sticking

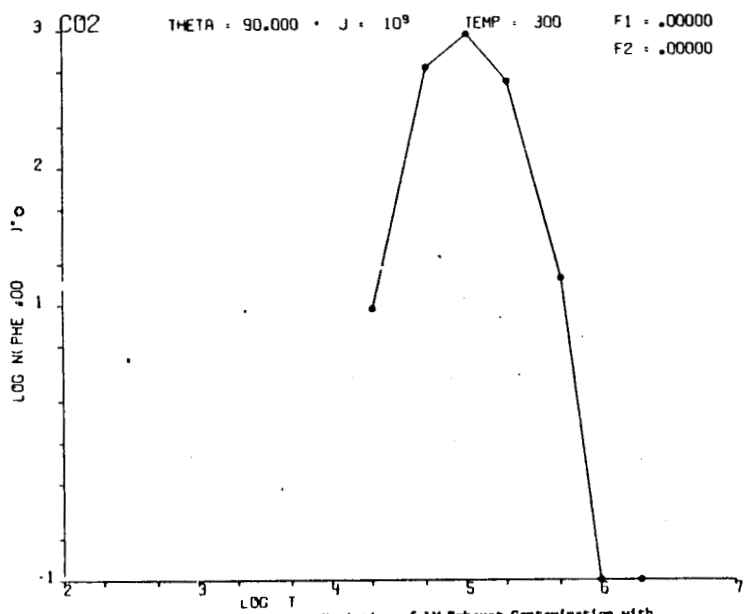

Fig. 29 CO_2 — Model II. Variation of LM Exhaust Contamination with Time (Log of Number of Particles/cm^3 versus Log of Time in Seconds) at 2700 km from LM Touchdown for No Sticking

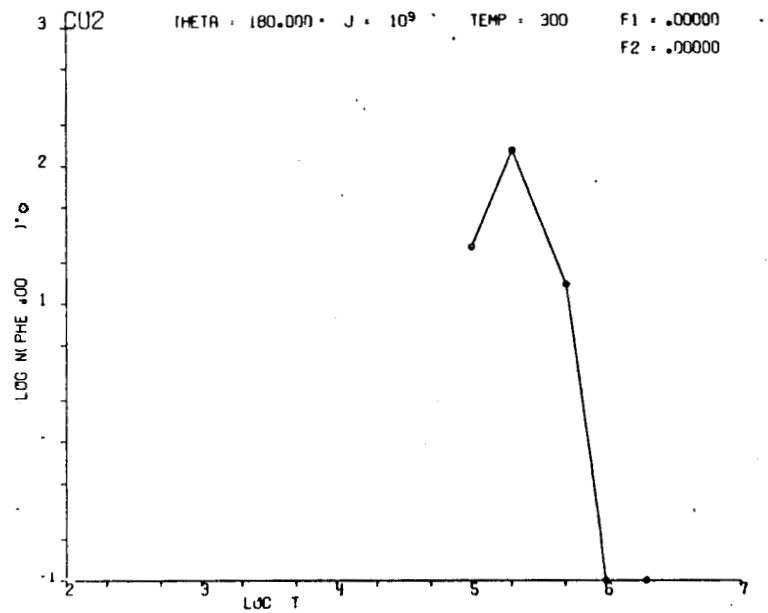

Fig. 30 CO_2 — Model II. Variation of LM Exhaust Contamination with Time (Log of Number of Particles/cm^3 versus Log of Time in Seconds) at 5600 km from LM Touchdown for No Sticking

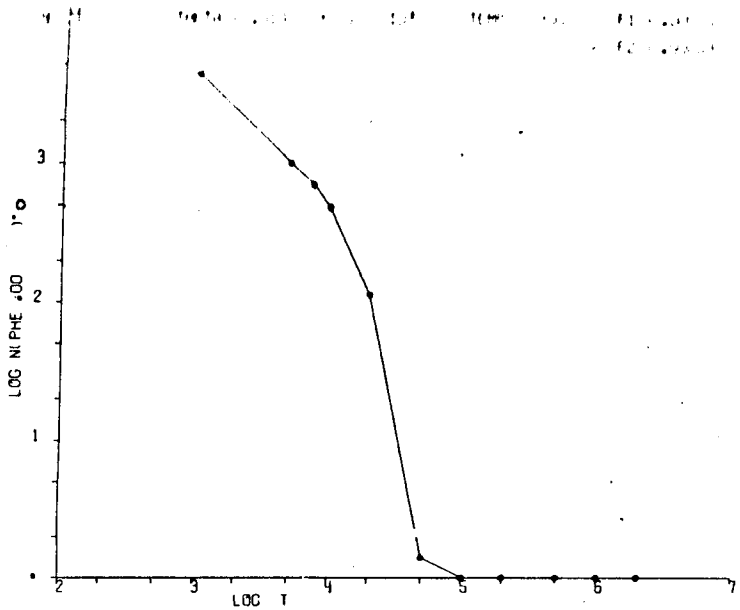

Fig. 31 H — Model II. Variation of LM Exhaust Contamination with Time (Log of Number of Particles/cm^3 versus Log of Time in Seconds) at 30 to 300 Meters from LM Touchdown for No Sticking

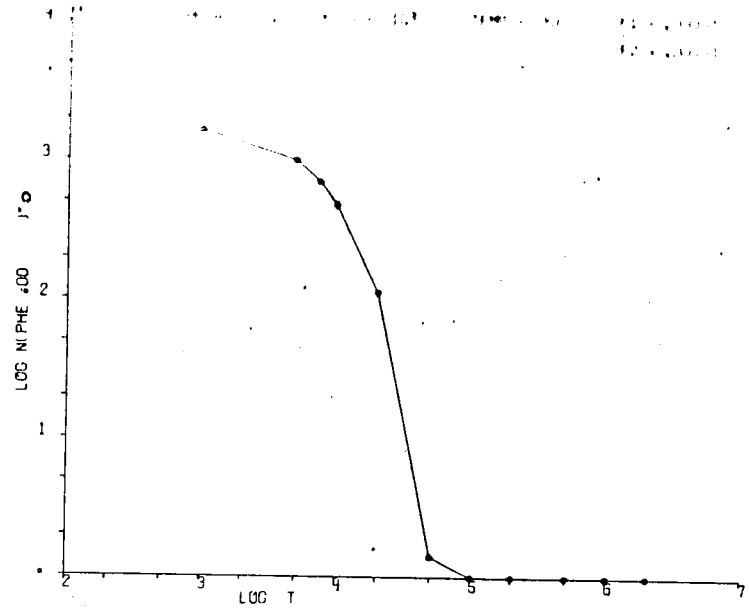

Fig. 32 H — Model II. Variation of LM Exhaust Contamination with Time (Log of Number of Particles/cm^3 versus Log of Time in Seconds) at 2700 km from LM Touchdown for No Sticking

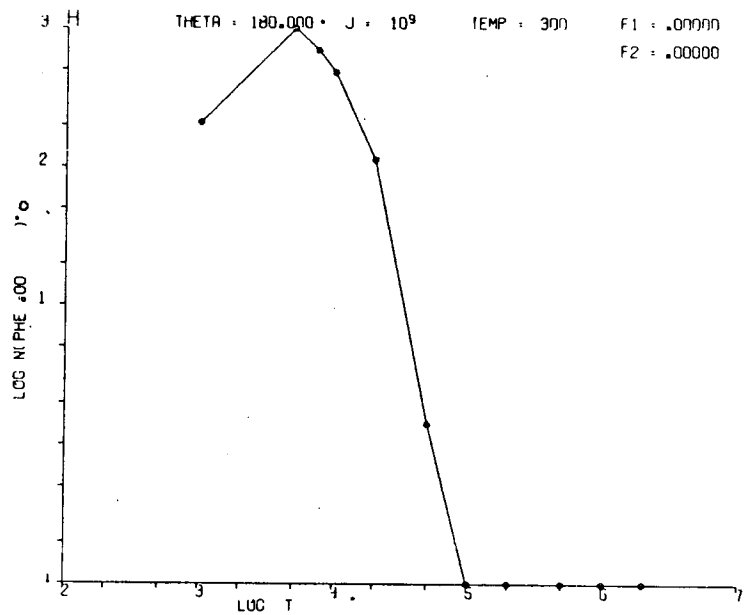

Fig. 33 H — Model II. Variation of LM Exhaust Contamination with Time (Log of Number of Particles/cm^3 versus Log of Time in Seconds) at 5600 km from LM Touchdown for No Sticking

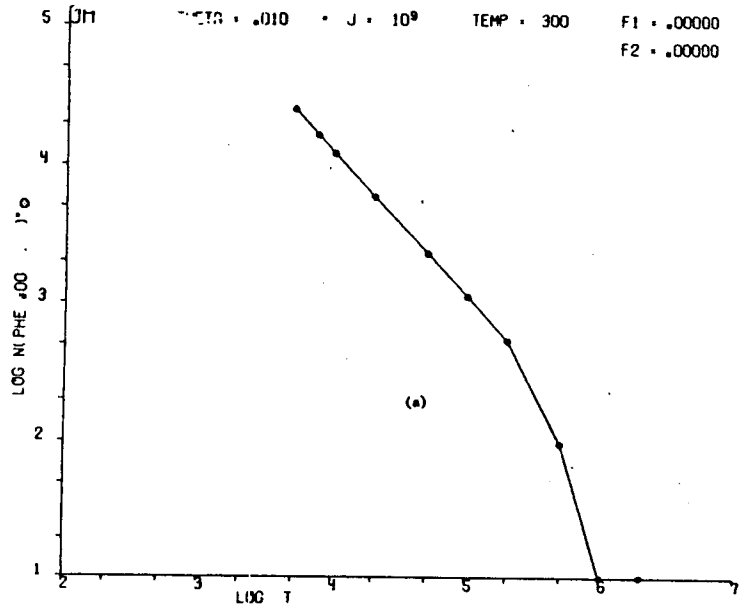

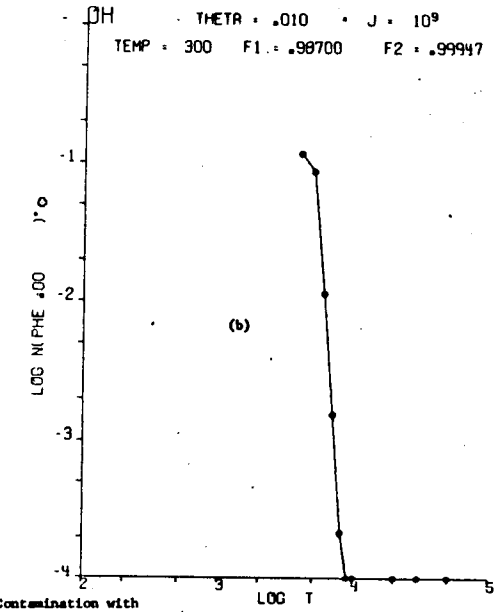

Fig. 34 OH — Model II. Variation of LM Exhaust Contamination with Time (Log of Number of Particles/cm^3 versus Log of Time in Seconds) at 30 to 300 Meters from LM Touchdown for (a) No Sticking, (b) Sticking

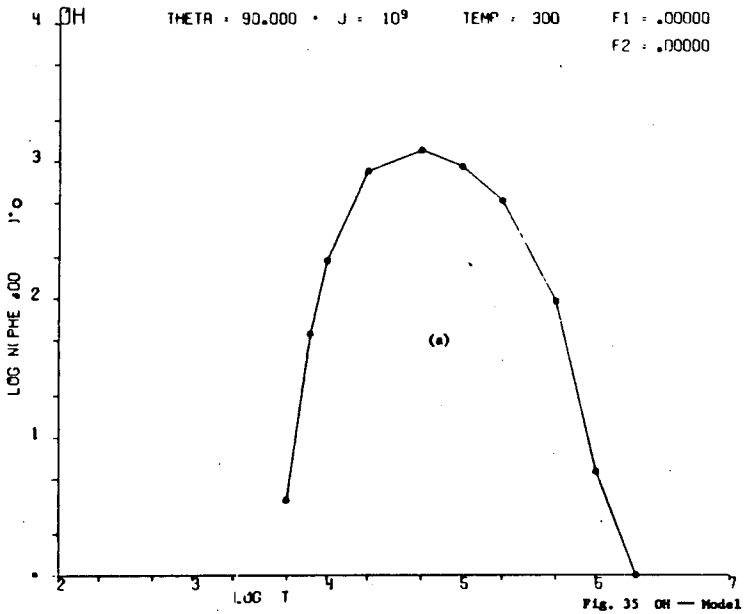

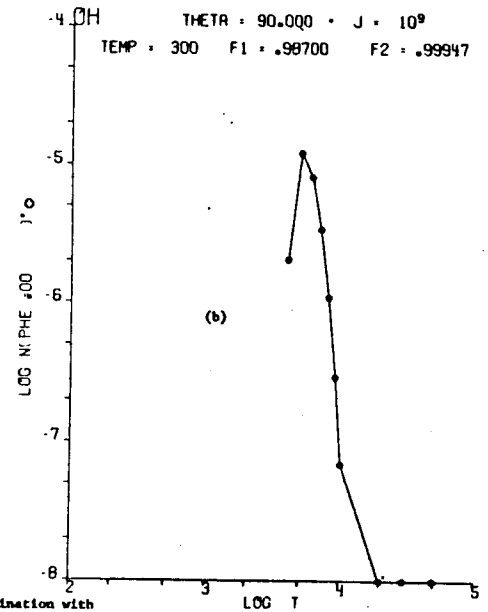

Fig. 35 OH — Model II. Variation of LM Exhaust Contamination with Time (Log of Number of Particles/cm^3 versus Log of Time in Seconds) at 2700 km from LM Touchdown for (a) No Sticking, (b) Sticking

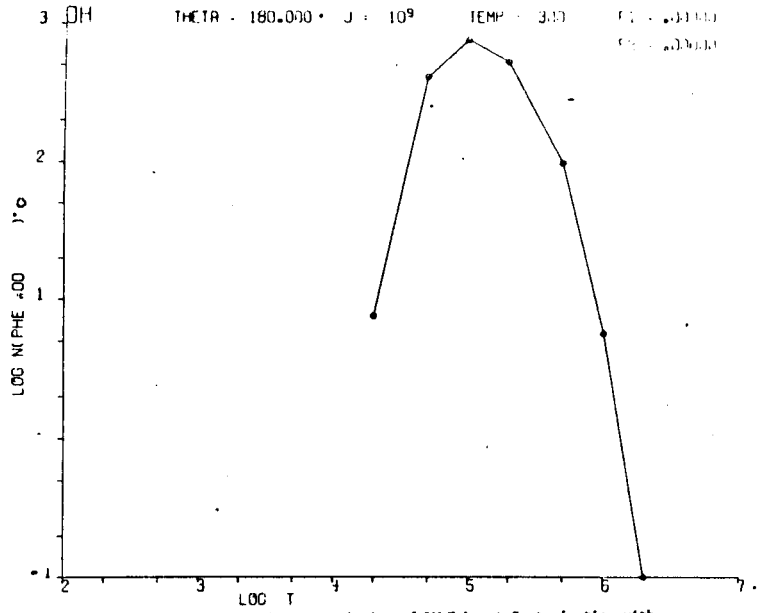

Fig. 36 OH — Model II. Variation of LM Exhaust Contamination with Time (Log of Number of Particles/cm^3 versus Log of Time in Seconds) at 5600 km from LM Touchdown for No Sticking

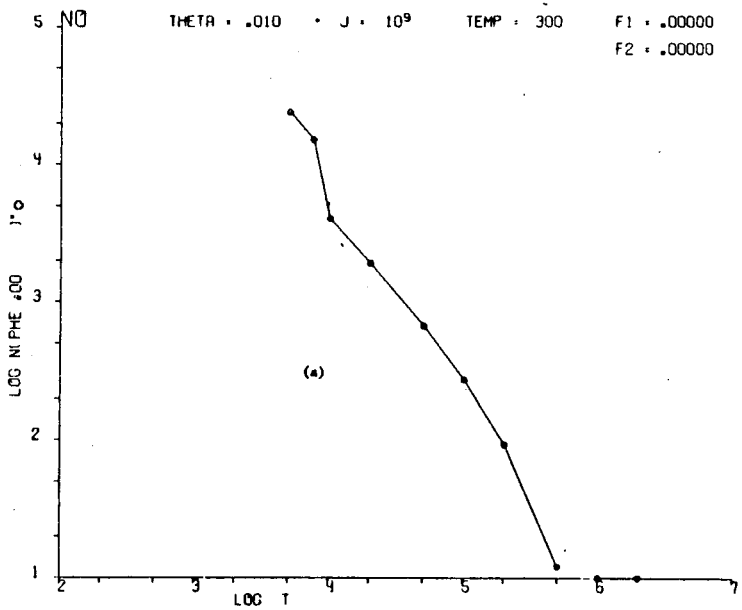

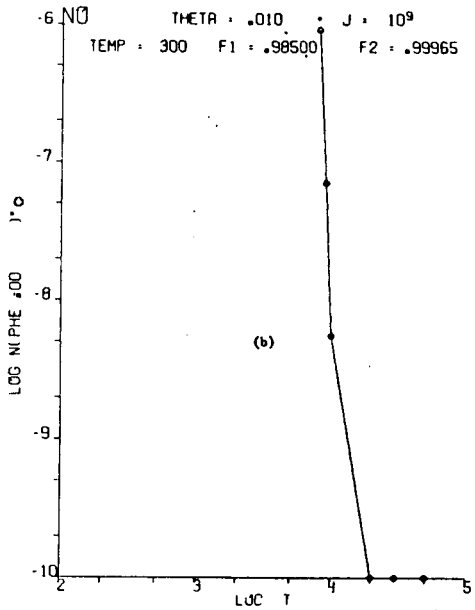

Fig. 37 NO — Model II. Variation of LM Exhaust Contamination with Time (Log of Number of Particles/cm^3 versus Log of Time in Seconds) at 30 to 300 Meters from LM Touchdown for (a) No Sticking, (b) Sticking

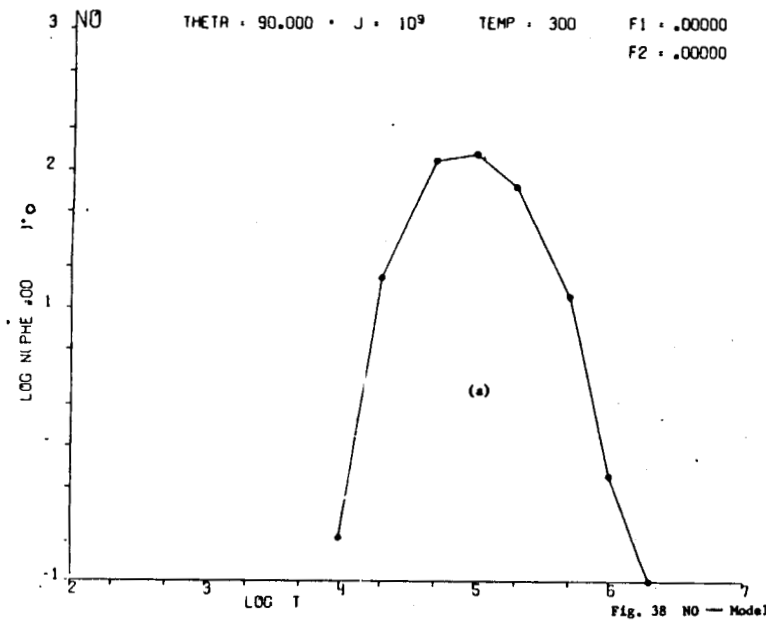

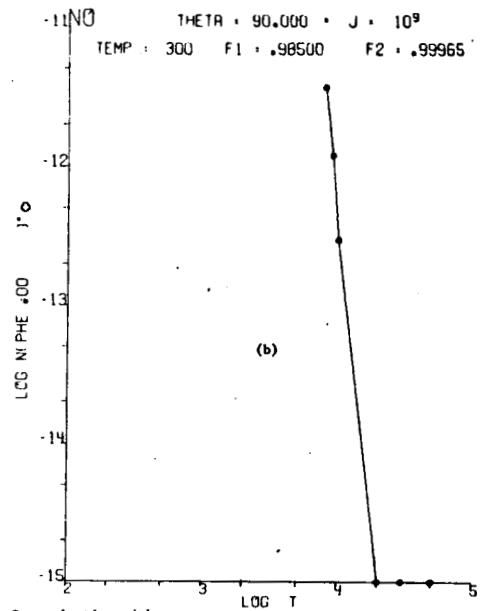

Fig. 38 NO — Model II. Variation of LM Exhaust Contamination with Time (Log of Number of Particles/cm^3 versus Log of Time in Seconds) at 2700 km from LM Touchdown for (a) No Sticking, (b) Sticking

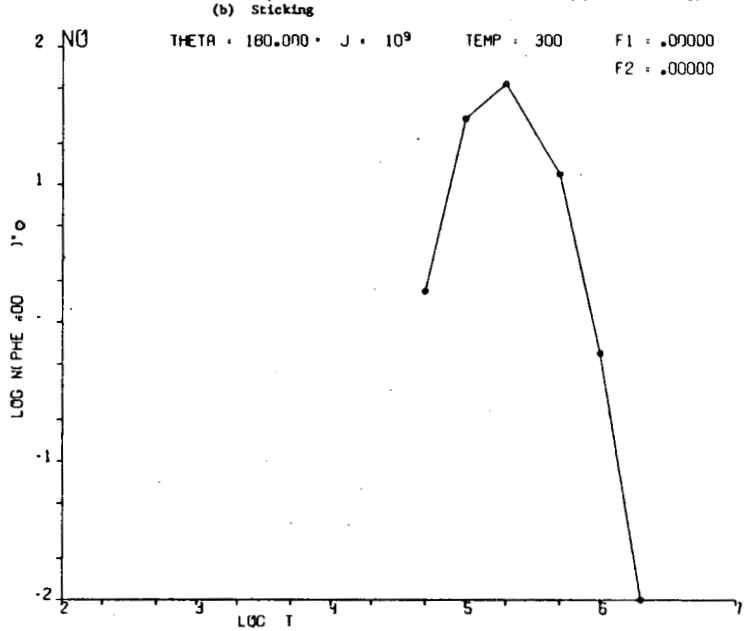

Fig. 39 NO — Model II. Variation of LM Exhaust Contamination with Time (Log of Number of Particles/cm^3 versus Log of Time in Seconds) at 5600 km from LM Touchdown for No Sticking

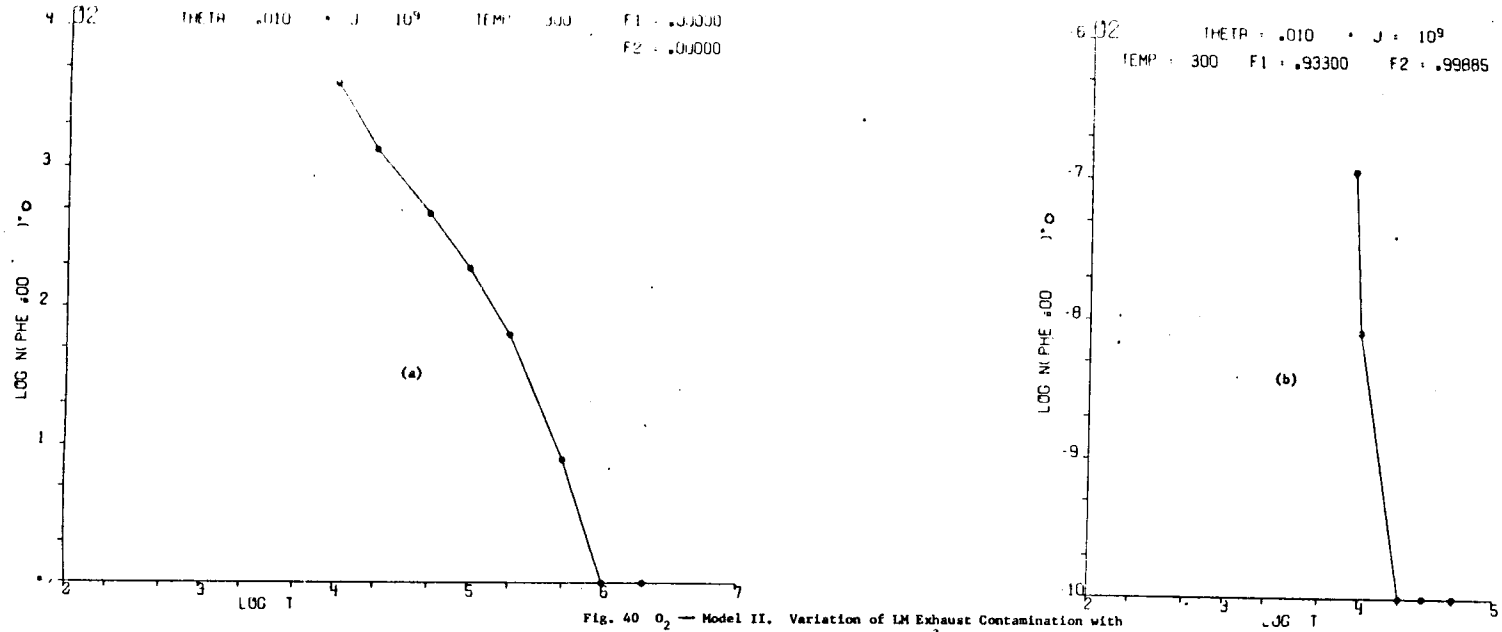

Fig. 40 O_2 — Model II. Variation of LM Exhaust Contamination with Time (Log of Number of Particles/cm^3 versus Log of Time in Seconds) at 30 to 300 Meters from LM Touchdown for (a) No Sticking, (b) Sticking

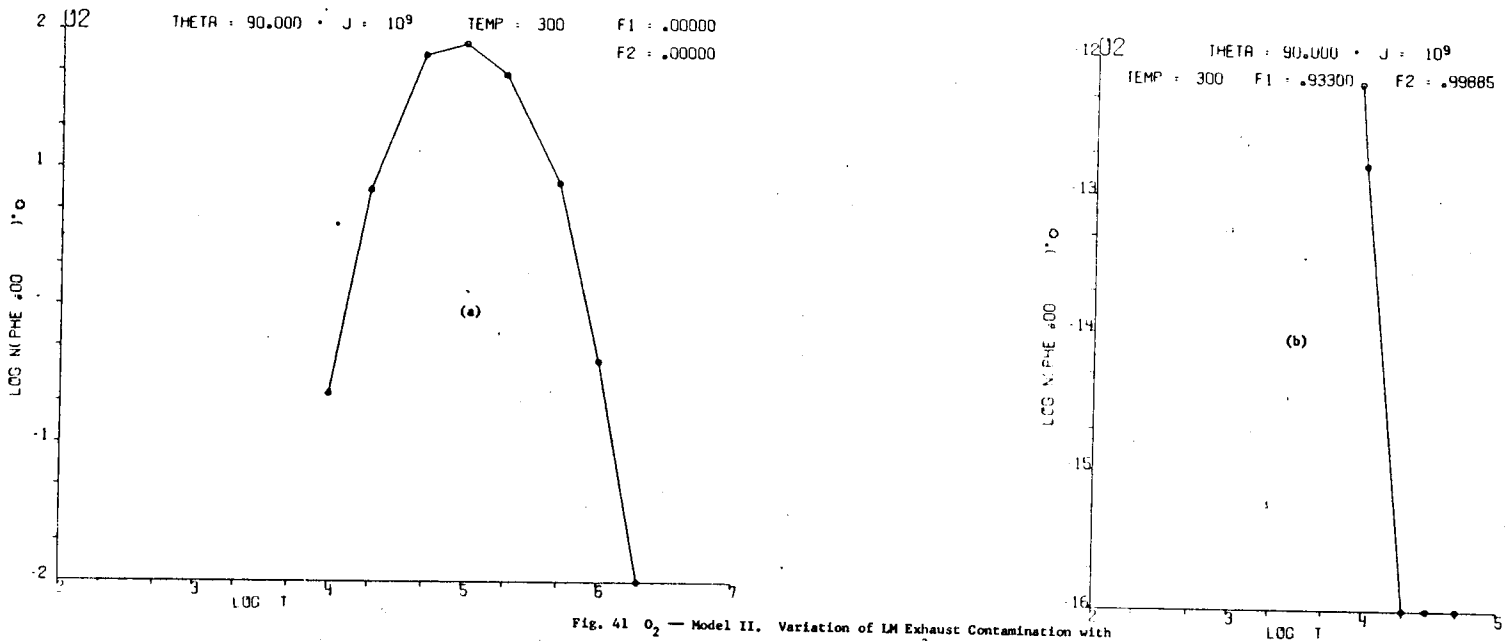

Fig. 41 O_2 — Model II. Variation of LM Exhaust Contamination with Time (Log of Number of Particles/cm^3 versus Log of Time in Seconds) at 2700 km from LM Touchdown for (a) No Sticking, (b) Sticking

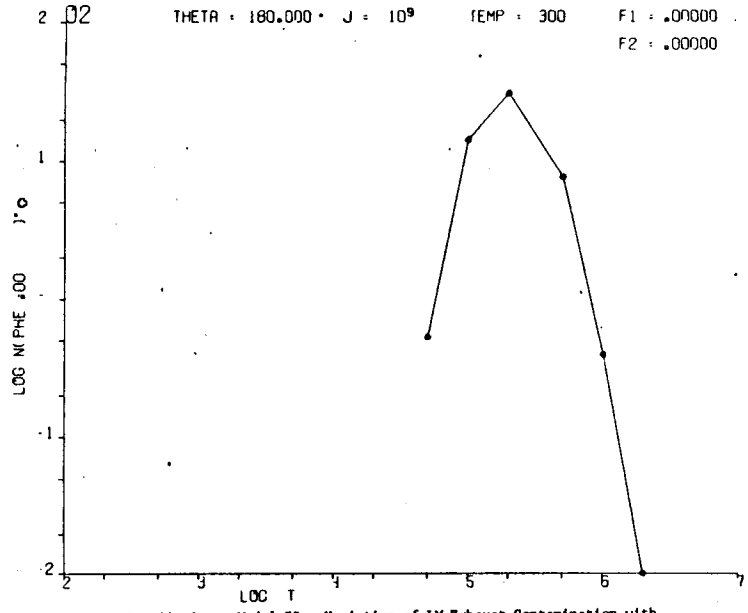

Fig. 42 O_2 — Model II. Variation of LM Exhaust Contamination with Time (Log of Number of Particles/cm^3 versus Log of Time in Seconds) at 5600 km from LM Touchdown for No Sticking

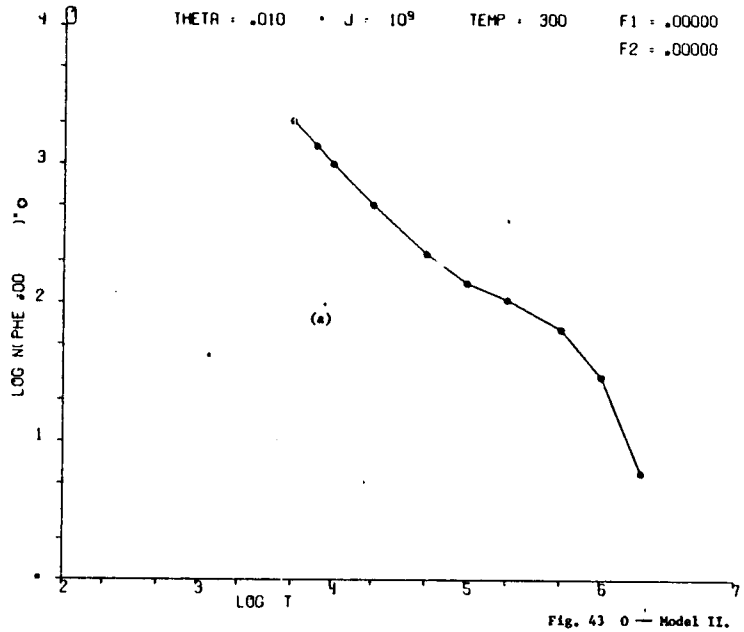

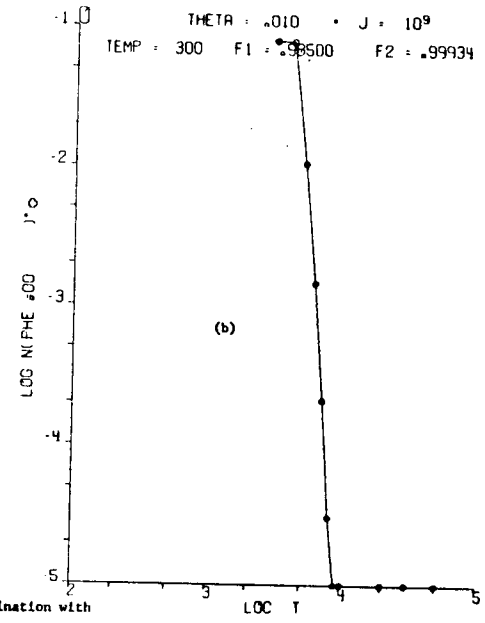

Fig. 43 O — Model II. Variation of LM Exhaust Contamination with Time (Log of Number of Particles/cm^3 versus Log of Time in Seconds) at 30 to 300 Meters from LM Touchdown for (a) No Sticking, (b) Sticking

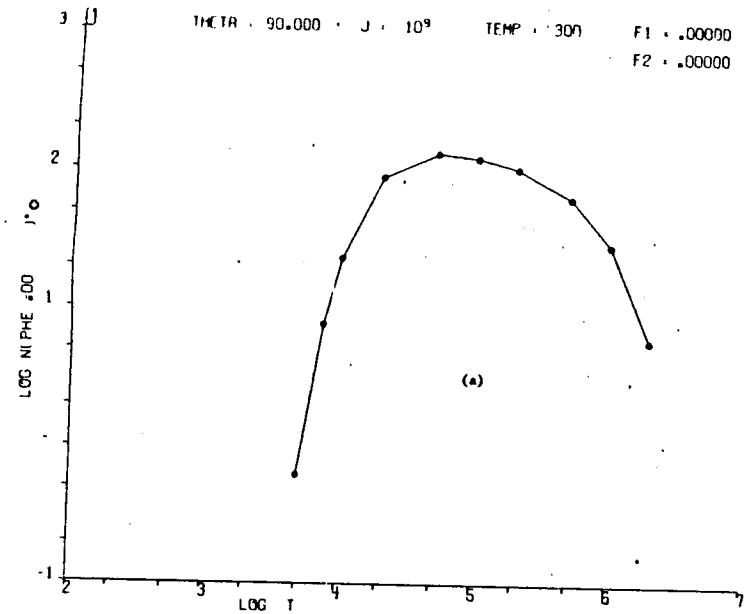

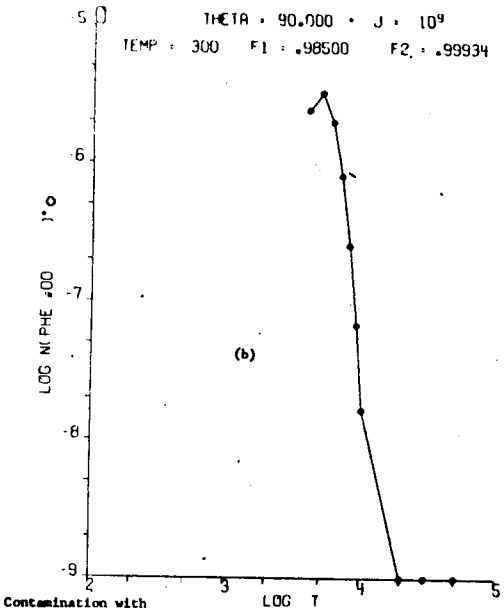

Fig. 44 O — Model II. Variation of LM Exhaust Contamination with Time (Log of Number of Particles/cm^3 versus Log of Time in Seconds) at 2700 km from LM Touchdown for (a) No Sticking, (b) Sticking

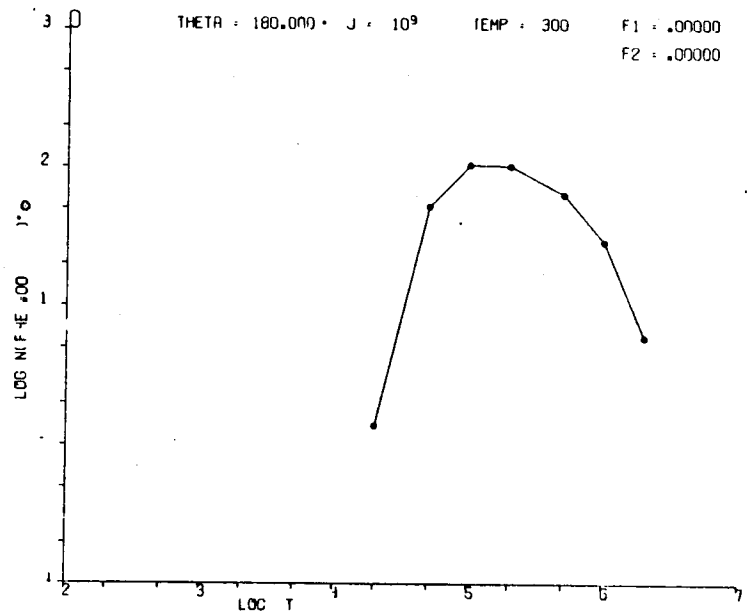

Fig. 45 O — Model III. Variation of LM Exhaust Contamination with Time (Log of Number of Particles/cm^3 versus Log of Time in Seconds) at 5600 km from LM Touchdown for No Sticking

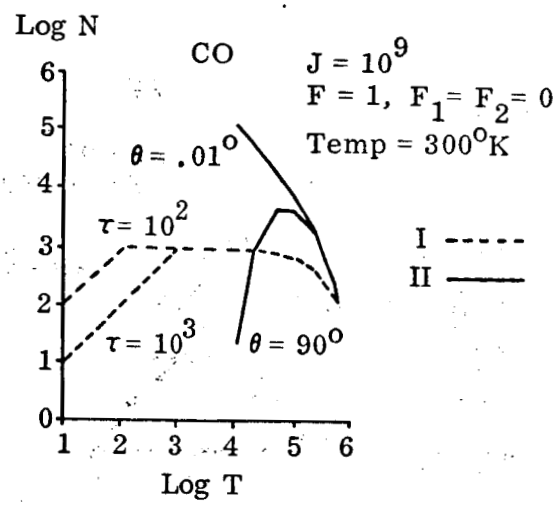

Fig. 46 Comparison of Model I Densities (Scaled Down by a Factor of 1/10) with Model II Densities for CO. No Sticking

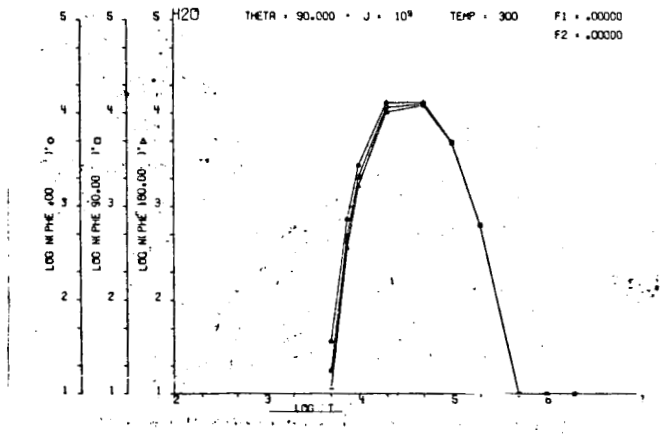

Fig. 47 Comparison of the Model II Densities of H_2O for Three Values of φ when $\theta = 90°$. No Sticking

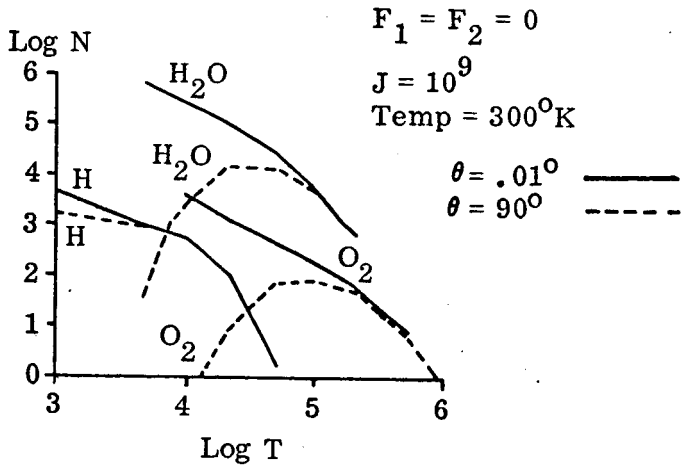

Fig. 48 Comparison of Model II Densities of H_2O, H, O_2 for $\theta = .01°$ with $\theta = 90°$. No Sticking

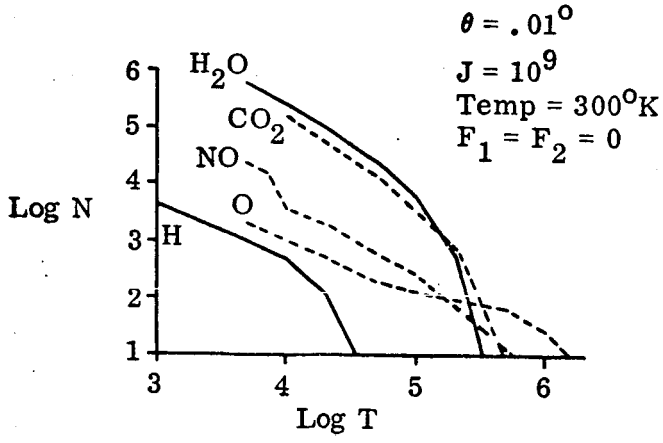

Fig. 49 Comparisons of the Variations with Time for Model II Densities of H_2O, CO_2, NO, O, H at $\theta = .01°$. No Sticking

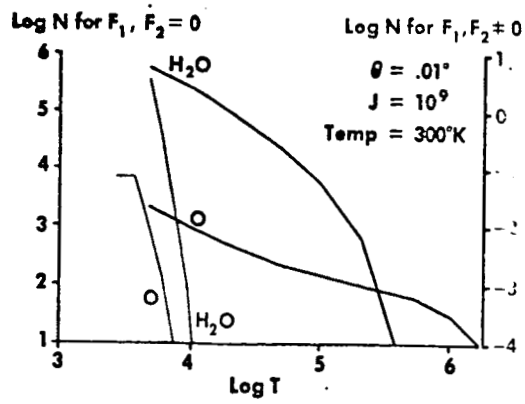

Fig. 50 Comparisons of Model II Densities of H_2O, O for the No Sticking with the Sticking Case at θ = .01°

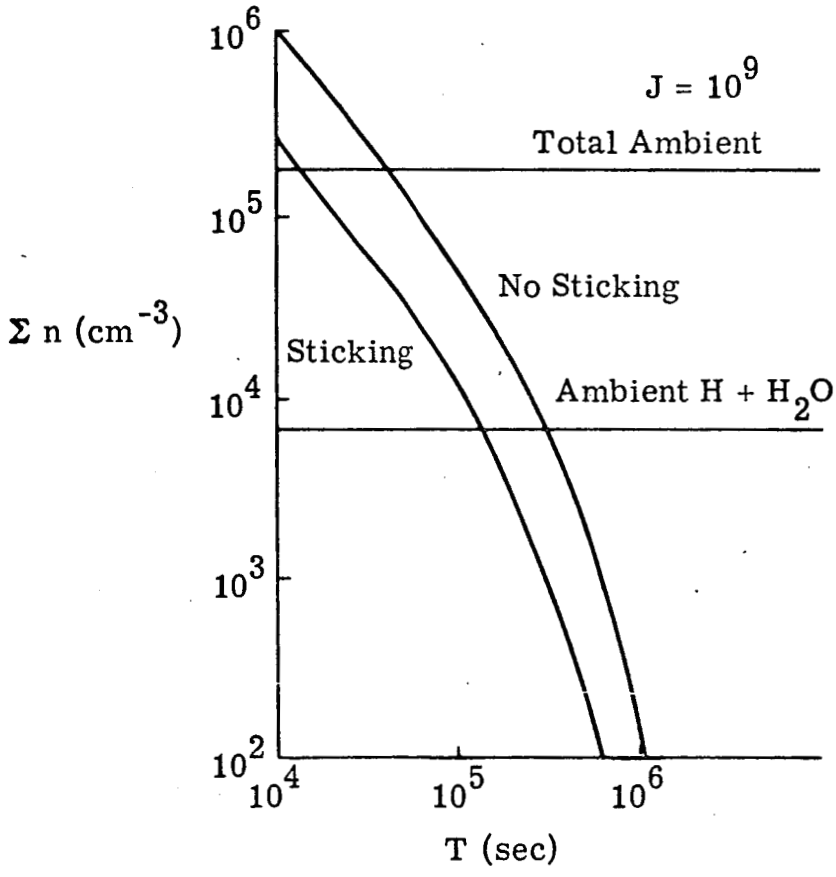

Fig. 51 Variation of Total Densities of Contaminants with Time at 30 to 300 Meters from LM Touchdown